Direct absorption transitions to highly excited polyads 8, 10, and 12 of methane

D. A. Sadovskií,[1,*] D. N. Kozlov,[2,1,†] and P. P. Radi[3,‡]

[1]*Département de physique, Université du Littoral Côte d'Opale, F-59140 Dunkerque, France*

[2]*A. M. Prokhorov General Physics Institute, Russian Academy of Sciences, 38 Vavilov St., 119991 Moscow, Russia*

[3]*Department of General Energy, Paul Scherrer Institute, CH-5232 Villigen PSI, Switzerland*

(Received 13 November 2009; published 6 July 2010)

We report on the experimental observation of high-resolution rotationally resolved spectra of vibrational polyads 10 and 12 of methane lying approximately halfway to the dissociation energy. The spectra were obtained at 295 K and 124 K and pressures as low as 200 mbar using a highly sensitive laser-induced grating (LIG) technique. The spectra correspond to direct single-photon absorption transitions from the ground state with cross sections as low as 10^{-25} to 10^{-26} cm^2 molecule^{-1}. We discuss theoretical developments toward the complete analysis of these transitions.

DOI: 10.1103/PhysRevA.82.012503 PACS number(s): 33.20.Tp, 33.15.Mt, 33.20.Kf

I. INTRODUCTION

Spectra of very weak absorption transitions long have been our principal source of information on specific molecular states or on conditions (pressure, temperature) in situations when usual dipole transitions are inaccessible (due to saturation, for example) or forbidden. Such are the well-known cases in planetary science, astrophysics, atmospheric observations, and plasma studies.

The weak absorption transitions that we study here are of a rather general nature. Their probabilities are extremely low not due to a specific property of the particular quantum molecular system (symmetry, spin, etc.) but because the absorbed photon increases the vibrational quantum number v associated with the affected vibrational degree(s) of freedom by a number of quanta $n \gg 1$, while in the usual allowed absorption transition v increases just by 1. For weak classical fields, the very small probability of such an event is described by the n-th Taylor series term of the effective dipole moment (see Sec. IV). These types of transitions with the maximal value $n_{\rm act}$ of the number of quanta of the dipole-active mode running as high as 6–7 were observed in a number of molecules, notably CO, CO_2, ozone, and methane (polyads P_n with $n = 2n_{\rm act}$)—all of great importance to various fields mentioned above as well as to molecular theory itself.

With recent advancements of spectroscopic techniques, it has become possible to reproduce these transitions *in vitro* at maximal spectral resolution. Thus in Ref. [1], we demonstrated the spectroscopic potential of the laser-induced grating (LIG) technique on the example of the $P_0 \rightarrow P_8$ near-IR transition of methane. Most recently, we observed similar transitions to polyads P_{10} and P_{12} [2]; see Fig. 1. The purpose of our article is to show how our and similar new experiments bring a standard spectroscopic study into the mainstream of the contemporary physics and to assess the theoretical work required for the satisfactory understanding of these data.

We realize that for a number of reasons, the required theory should go significantly beyond standard techniques of molecular spectroscopy and that a detailed traditional line-by-line analysis and a spectroscopic fit to a Taylor series phenomenological model may be but a very distant possibility. The main issue is in preparing the foundation for such a future analysis. Typically, spectroscopists base their description on small groups of vibrational states which they can describe by reasonably compact phenomenological models. The classification of the states begins with the ground state, i.e., the framework of small vibrations about the equilibrium is assumed. We cannot continue this scheme to the states involved in our experiments. Figuratively speaking, we should find instead a different starting point for the series approximation. We believe that this point can be found by replacing "static" equilibrium-based linear vibrational normal mode theory for dynamical nonlinear analysis that can select stable highly nonlinear localized vibrations. Though the idea itself is not entirely new, we like to draw more attention to this problem and to set up the framework of thinking that may lead to a satisfactory physical explanation and the eventual quantitative analysis.

A. Vibrational levels of methane

Methane (CH_4) is a light highly symmetric five-atomic molecule. The spatial symmetry group of its rovibrational Hamiltonian is the tetrahedral group[1] T_d of order 24; the full symmetry group $T_d \times \mathcal{T}$ [3] which includes time-reversal $\mathcal{T}$ is isomorphic to O_h. This group has two important classes of subgroups which we refer to as D_{2d} and C_{3v} and which are built around fourfold and threefold axes, respectively; see Fig. 2. Methane has nine vibrational degrees of freedom combining into four vibrational normal modes: ν_1 (of symmetry type A_1, or the fully symmetric mode), ν_2 (E), ν_3 (F_2), and ν_4 (F_2); ν_1 and ν_3 are stretching modes, ν_2 and ν_4 are bending modes. The ratio of the harmonic frequencies of these modes

$$\omega_1 : \omega_2 : \omega_3 : \omega_4 \approx 2 : (1{:}1) : (2{:}2{:}2) : (1{:}1{:}1) \qquad (1)$$

*sadovski@univ-littoral.fr

†dnk@kapella.gpi.ru

‡peter.radi@psi.ch

[1]Recall that cubic groups have irreducible representations of dimension 1, 2, and 3, denoted A, E, and F, respectively.

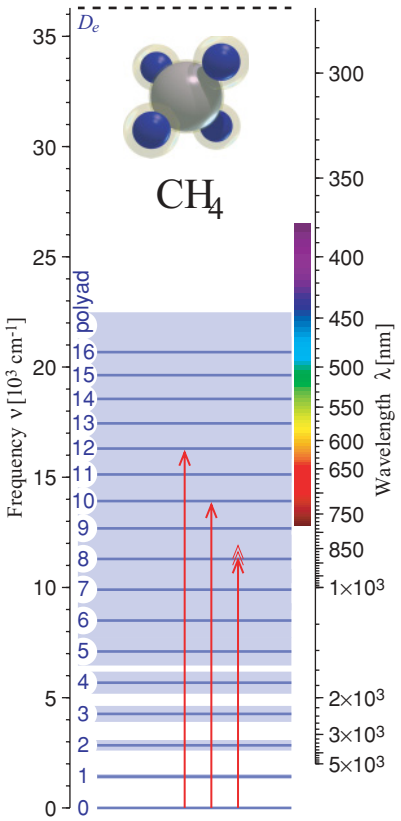

FIG. 1. (Color online) Polyads of methane and transitions discussed in this work.

is typical for small molecules and can be considered as a multidimensional Fermi resonance. Due to this resonance, quantum vibrational states with the same

$$n = 2n_1 + n_2 + 2n_3 + n_4, \tag{2}$$

where n_k is the number of quanta in mode k, form quasidegenerate *polyads* P_n labeled by polyad quantum number n. Vibrational polyads exist in many molecules (CO_2, C_2H_2, H_2O, etc.). The specifics here is in the presence of several degenerate vibrations which may be considered as exact resonances. Such highly degenerate situation exacerbates the problem of classifying and selecting desired states within a polyad. The analysis is certainly made quite complicated due to the large total number $K = 9$ of vibrational degrees of freedom involved. This kind of studies is more common for $K = 2$ or 3 where we can rely more on physical intuition. Furthermore, the high symmetry of the system imposes the use of certain mathematical methods which are less important in other systems. These technical detals can be found elsewhere [3,4] and we keep them to a minimum.

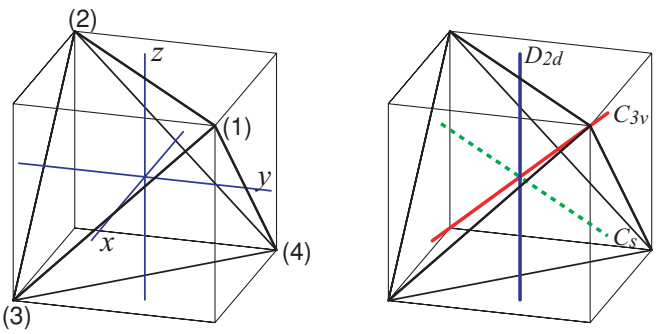

FIG. 2. (Color online) Coordinates in $\mathbb{R}^3$ and symmetry axes of a tetrahedron.

The ground state of methane P_0 and the first two polyads,[2] the *dyad* P_1 and *pentad* P_2, have been studied extremely well [4–6]. P_1 is formed by bending fundamentals ν_2 and ν_4, while pentad includes stretching fundamentals ν_1 and ν_3, and bending overtones $2\nu_2$, $\nu_2 + \nu_4$, and $2\nu_4$. The analysis of the *octade* P_3, can still be regarded as sufficiently complete [7,8], and very satisfactory progress has been made in the study of P_4 which includes first overtones and combinations of stretching modes: $2\nu_1$, $\nu_1 + \nu_3$, and $2\nu_3$. Higher polyads remain a widely open field. The number of rotational levels there is so large that their complete assignment can hardly be imagined at present. At the same time, the potential well of methane is very deep, and even polyad P_{10} situated at about 14 000 cm^{-1} is not even halfway to the first dissociation energy D_e of approximately 35 000 cm^{-1} (for CH_3-H) [9]; see Fig. 1.

In the past decade, extensive computations [10–15] have been attempted in order to climb up this vibrational potential in various ways. However, the analysis of the actual dynamics of this excited system with strongly interacting nine degrees of freedom did not follow. It is likely that the concepts of relative equilibrium and nonlinear normal mode[3] generalizing the more intuitive and simple molecular ideas of local mode and chromophore, are still not fully apprised in molecular physics. Yet it is on these more general and truly dynamical concepts that our progress depends entirely in the case of methane.

B. Spectra and their tentative assignment

We survey briefly what has been done before us. Since the mid-1990s, a variety of methods has been developed and applied for extended high-resolution and low-rotational-temperature investigations of weak overtone and combination absorption transitions to the high-lying vibrational states of methane. In particular, three features of the methane spectrum have been observed in the near-IR spectral range of 889, 861, and 840 nm (between 11 170 and 11 980 cm^{-1}). These bands are the most prominent features of the $P_0 \rightarrow P_8$ transition. Intracavity photoacoustic and tone-burst modulation spectroscopy [21–23], and intracavity laser absorption [24], were used to study methane bands around 11 300 cm^{-1}. In addition, the high sensitivity of the intracavity laser absorption technique has been employed to measure absorption spectra and coefficients between 10 635 and 13 300 cm^{-1} [25]. Later, the spectral region around 11 900 cm^{-1} has been investigated

[2]The names dyad, pentade, etc., reflect the number of normal mode components—not the actual total number of vibrational states. So, taking the degeneracies into account, the respective numbers of states in the dyad and pentade are 5 and 19.

[3]Nonlinear normal modes were introduced in Refs. [16–18], and a more concrete molecular application was given in Ref. [19]. Within the polyad framework, they were treated later as relative equilibria [3,20].

by applying wavelength-modulated diode laser spectroscopy [26]. Recently in Ref. [1], we have applied LIG spectroscopy, a nonlinear technique using resonances of linear absorption, for the investigation of these absorption bands with resolution of about 0.04 cm^{-1}.

The most prominent band of the $0 \rightarrow P_8$ spectrum at 889 nm is similar to the P_{10} and P_{12} transitions that we describe here in Sec. II. The presence of this relatively simple and compact strong band is striking. This band is tempting to be assigned as a transition to a single vibrational "bright" upper state, which Giver [27] and later Boraas *et al.* [21] assigned tentatively as the $3\nu_1 + \nu_3$ stretching combination overtone strongly coupled to several "dark" close-lying states. The weaker 861 and 840 nm features were attributed to the combination bands $2\nu_1 + 2\nu_3$ and $\nu_1 + 3\nu_3$, respectively. This assignment persisted in later work [22–26].

Admittedly, the $3\nu_1 + \nu_3$ normal mode assignment simplified the spectroscopic analysis because the rotational structure of the $0 \rightarrow 3\nu_1 + \nu_3$ transition resembles that of the $0 \rightarrow \nu_3$ fundamental. However, the presence in P_8 of such a predominantly stretching normal mode overtone seems unlikely because of strong couplings between the modes. Thus already in P_4, the stretching overtones $2\nu_1$, $\nu_1 + \nu_3$, and $2\nu_3$ have the respective normal mode content at the level of only 70% (see Table IV in Ref. [7]) and this percentage drops quickly in higher polyads.[4] So, more generally, we may interpret the bright P_8 state as a *localized vibrational state* (of predominantly stretching nature if we want to accommodate for Ref. [21–23]).

Unlike its cousins with heavier central atom (Si, Ge) [20,28–31], methane is not known to have true *local mode* states [10,12,13]. It may, nevertheless, have vibrational localization of a more complex, dynamical nature. So *our immediate goal* is to understand whether vibrational localized states of any kind, and purely stretching ones in particular, can show up in highly excited polyads of methane (see more in subsection II C).

II. OBSERVED SPECTRA

In this work, we present higher frequency absorption spectra of methane recorded using the LIGs technique in the 727-nm (Fig. 3) and 619-nm (Fig. 4) regions, corresponding to the transitions $P_0 \rightarrow P_{10}$ and $P_0 \rightarrow P_{12}$, respectively [2]. Following the tradition, one may like to assign these spectra to combination bands $4\nu_1 + \nu_3$ and $5\nu_1 + \nu_3$.

A. Laser-induced gratings

In general, laser-induced gratings are spatially periodic variations of the complex refractive index of the medium. General information on LIGs in various media can be found in Ref. [1] and references therein. If molecules are resonantly excited by a short-pulse radiation in the interference region of two pump laser beams at wavelength λ_p, which are crossed at angle $2\theta_p$, a spatially periodic variation of the population

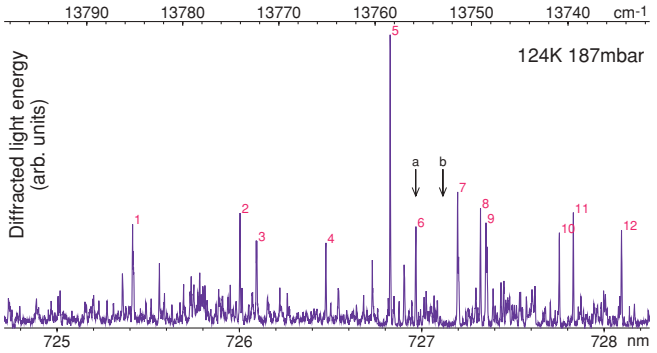

FIG. 3. (Color online) The central part of the LIG absorption spectrum [2] of the $P_0 \rightarrow P_{10}$ transition in methane recorded at 124 K and 187 mbar with spectral resolution of 0.04 cm^{-1}; the "zero signal" level coincides with the nm axis. The arrows (a) and (b) point to the pump wavelengths λ_p for the resonant and nonresonant signal temporal profiles in Fig. 5.

of the energy levels involved is produced. The period of the spatial modulation equals to the interference fringe spacing, $\Lambda = \lambda_p/(2 \sin \theta_p)$. Fast collisional deactivation of the excited states may provide a corresponding modulation of the refractive index resulting from local temperature and density variations and thus lead to the formation of so-called *thermal* LIGs. Adiabatic compression of the gas by the spatially inhomogeneous pump electromagnetic field strength, simultaneous with resonant excitation, generates nonresonant *electrostrictive* LIGs. LIGs are usually registered by detecting the part of read-out laser radiation which crosses the pump beams interaction region and is diffracted by the modulations

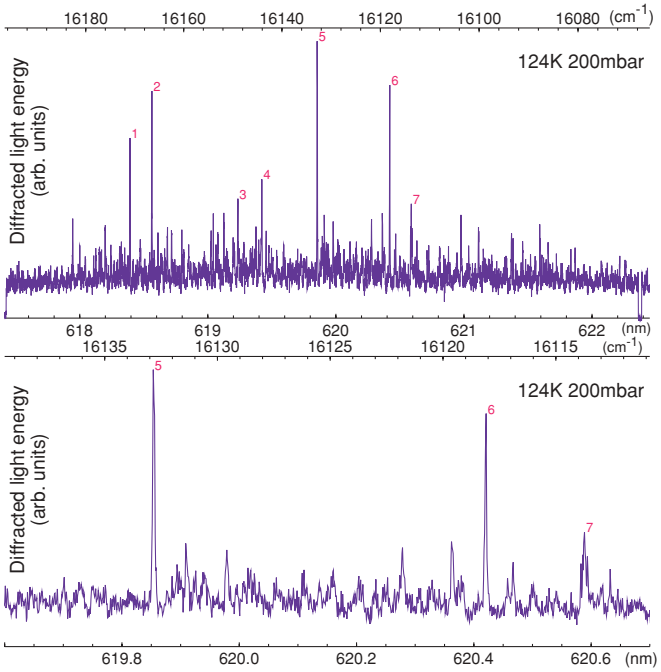

FIG. 4. (Color online) The central part (top) and its blowup (bottom) of the LIG absorption spectrum [2] of the $P_0 \rightarrow P_{12}$ transition in methane recorded at 124 K and 200 mbar with spectral resolution of 0.04 cm^{-1}; the "zero signal" level coincides with the nm axis.

[4] V. Boudon, private communication on the computation for $0 \rightarrow P_8$ using currently known spectroscopic Hamiltonian of methane.

TABLE I. Principal features of direct absorption transitions to polyads 10 and 12 of methane at low temperature [2]. Line numbers correspond to those indicated in Figs. 3 and 4; respectively, line intensities I are given in relative units.

$P_0 \rightarrow P_{10}$			$P_0 \rightarrow P_{12}$		
No.	λ (nm)	I	No.	λ (nm)	I
1	725.414	35	1	618.392	67
2	726.003	39	2	618.563	83
3	726.095	29	3	619.234	46
4	726.474	29	4	619.421	52
5	726.826	100	5	619.853	100
6	726.967	34	6	620.420	85
7	727.196	46	7	620.588	44
8	727.322	40			
9	727.352	36			
10	727.754	32			
11	727.831	39			
12	728.095	33			

of the complex refractive index. For efficient diffraction, the read-out, or probe beam, at wavelength λ_r, should be directed to the planes of the fringes at the Bragg angle θ_r, defined as $\sin\theta_r = \lambda_r/(2\Lambda)$. If a continuous-wave (cw) probe radiation is employed, the temporal evolution of diffraction efficiency of a short-pulse excited LIG can be recorded. A pulse of the diffracted light registered by a photodetector generates the characteristic LIG signal $S(t)$.

A typical resonant signal observed in the $P_0 \rightarrow P_{10}$ band of CH_4 (at 187 mbar and 124 K) is presented in Fig. 5(a). It was recorded after tuning the pump wavelength λ_p to the resonance with the transition at 726.967 nm (line 6 in Fig. 3 and Table I). The signal oscillations in this figure correspond to the variations of the refractive index caused by spatially periodic acoustic waves and stationary density modulations. Both are induced by rapid collisional deactivation of the excited CH_4 molecules, and the signal's temporal profile is characteristic

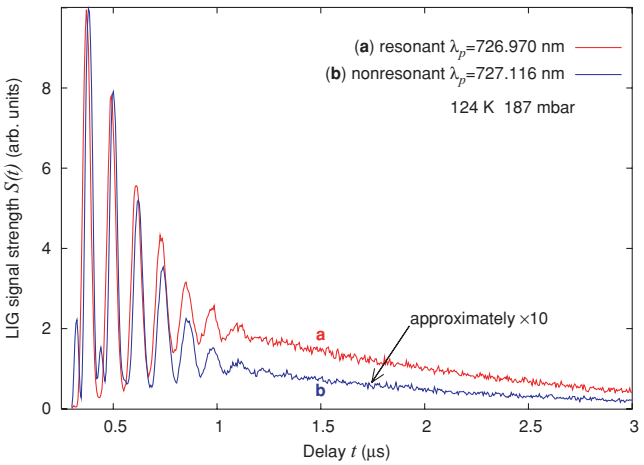

FIG. 5. (Color online) Typical temporal profiles of the LIG signals recorded in the $P_0 \rightarrow P_{10}$ band of CH_4 (187 mbar, 124 K, cf Fig. 3) for (a) resonant excitation at pump wavelength $\lambda_p = 726.967$ nm (line 6 in Fig. 3 and Table I) and (b) nonresonant excitation at $\lambda_p = 727.116$ nm in the region of weak absorption.

for that determined by the thermal LIGs. The period of the oscillations of about 120 ns and the signal decay scale of a few microseconds are determined by the fringe spacing Λ and the sound velocity. Spectroscopy of the absorption transitions is accomplished by means of tuning the pump laser frequency through the range of interest and measuring the peak value of $S(t)$, or its integral within a definite time interval, as a function of frequency.

B. Experimental details

The experimental setup employed in this work has been described previously [1]. In brief, the output radiation of a 20-Hz repetition rate narrowband tunable dye laser providing up to 25 mJ/pulse was employed as a pump source. Pulse duration was approximately 10 ns and a spectral bandwidth was ≈0.04 cm^{-1}. The dye laser was pumped by the frequency-doubled radiation of a Nd:YAG laser. To obtain coherent radiation in the near-infrared region of 835–895 nm, the frequency of the dye laser was Raman shifted in a 1.5-m-long cell containing H_2 at 5 bar. The pump radiation was split into a pair of roughly equally intense LIG excitation beams with parallel polarizations. These beams were subsequently focused by a lens ($f = 900$ mm) and intersected at the crossing angle of $2\theta_p \approx 1.20^\circ$ (see Fig. 6) that provides a fringe spacing of $\Lambda \approx 35$ μm at $\lambda_p = 727$ nm. A wavemeter with the specified accuracy of 10^6 is used to measure the absolute excitation wavelength in each pulse.

The LIGs are read out by utilizing the beam of an Ar^+ laser delivering up to 1.1 W at 514.5 nm. The cw probe beam is propagating parallel to the pump beams and focused by the same lens into the interaction region at a Bragg angle of $\theta_r = 0.42^\circ$. In this manner, a 3D forward phase-matching geometry is arranged (see Fig. 6). The diffracted light is spatially filtered and coupled into a multimode fused silica fiber delivering it to a fast photomultiplier. Additional stray-light reduction is achieved by using a band-pass interference filter centered at the read-out laser wavelength and placed in front of the photomultiplier. Temporally resolved acquisition of the LIG signals, single-shot or averaged, is performed by using a digital oscilloscope with an analog bandwidth of 1 GHz and a sampling rate up to 4 gigasamples/s. The signals are recorded during 2–10 μs, depending on pressure. Spectra are obtained by scanning the frequency of the dye laser radiation and accumulating the LIG signal integrated within an

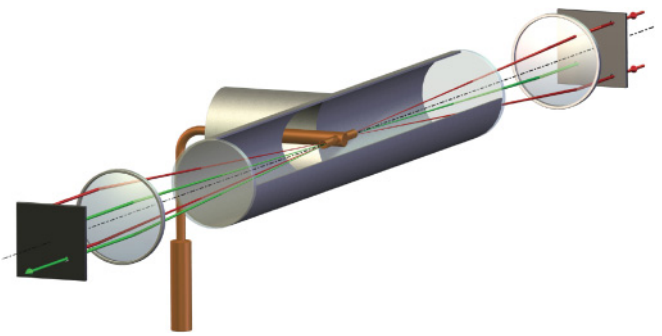

FIG. 6. (Color online) The focusing geometry of the pump, probe, and signal beams in the LIGs experiment; the gas cell with the cold finger are represented schematically.

optimized time interval after the excitation pulse. The spectral resolution of about 0.04 cm^{-1} has been provided.

The gas cell used in our experiments could be evacuated to less than 10^{-4} bar and allowed to work with gas pressures up to 5 bar. Gas pressure in the sample volume was measured by a capacitance manometer. A copper cold finger cooled by liquid nitrogen was mounted to enter into the cell (see Fig. 6). The sample volume, with the dimensions of about 0.3 mm in diameter and 20 mm in length, was located at the axis of a narrow (5 mm in diameter and 30 mm in length) channel through the cold finger. The channel wall temperature was measured by a thermocouple. The measurements in the gas cell were performed at CH_4 pressures of 0.2–4 bar and temperatures 298 K and 124–130 K. Methane of quality 2.5 (Messer-Griesheim) has been used for the measurements.

C. Spectra and their assignment: The main objective of the work

In the rotational structure of spectra $P_0 \to P_n$ with $n = 8,10,12$, we distinguish immediately two kinds of lines: a relatively small number of prominent lines (Table I) forming a 100–200 cm^{-1} (several nm's at these frequencies) large band and a very dense broader "undergrowth" of much weaker numerous overlapping lines (see Figs. 3 and 4). All these lines rise above a structureless background which can be particularly well observed in Fig. 4 where the actual zero-absorption signal level is coincident with the nm axis. To study the background, we tuned the pump frequency away from single sharp lines and recorded the temporal profiles of the LIG signal. From these experiments [see Fig. 5(b)], we can conclude that the background signal, though being about an order of magnitude weaker and hence demonstrating noticeable nonresonant contribution from the electrostrictive LIG (seen as smaller oscillation peaks), is nevertheless caused primarily by the thermal LIGs which result from the *resonant* absorption of the pump radiation.

The conclusion, plausible to anyone familiar with the rotation-vibration bands of methane, is that the prominent lines represent rotational levels of one single or, at most, a few "bright" vibrational states, while the weaker lines *and* the background result from a very dense spectrum of surrounding "dark" states coupled to the bright ones through various vibrational and rovibrational mechanisms.

In order to simplify the spectra and to facilitate the eventual identification of the spectral lines, we attempted to reduce the number of the populated rotational ground state levels by the cryogenic cooling of the small sample volume in the middle of the gas cell (see Fig. 6) down to temperatures $T \approx 120$ K. Note that the angular momentum $J_{\max}$ of the most populated rotational ground-state level of CH_4 can be estimated as $J_{\max} \approx \sqrt{kT/hcB}$, where $B \approx 5.24$ cm^{-1} is the rotational constant of the molecule. So lowering T from 295 K to 124 K brought $J_{\max}$ down from 6 to 4. We have also observed, that the number of the strongest visible lines in the cold gas spectra appears to decrease with growing polyad number n (or pump radiation frequency).

The dense spectrum of the second kind is expected. Indeed, at these excitation energies, just the density of vibrational states is approximately one or several states per cm^{-1}, the splittings are less than characteristic interaction terms, and all these states are typically mixing well with each other. We are in the semiclassical domain and the dynamics of the classical limit system at these energies is significantly irregular.

On the other hand, the existence of such a relatively small number of very bright states is fascinating. How is it possible for the specific absorption process to be so selective? There are two aspects to this question: the nature of the excited state and the absorption process itself. We address them in Secs. III and IV, respectively. Both aspects surpass considerably the domain of a traditional spectroscopic study. Answering the first part involves analyzing possibilities of regular motions in a strongly perturbed nonlinear dynamical system with many degrees of freedom and the corresponding localization in the quantum analog system. The second part requires detailed understanding of the specific interaction of such a system with light under essentially semiclassical conditions.

III. VIBRATIONAL POLYADS OF METHANE

We turn to the first part of the question: what subset of the vibrational states of the polyad P_n is involved in the observed transitions $P_0 \to P_n$ with large $n = 8,10,12$? Is it a small group of well-localized excited states? If yes, what is its nature? If no, why is the rotational structure of the spectrum so "simple"? After recalling pertinent details of the polyad theory in subsection III A, we address these questions in subsection III C. The theory in subsections III A and III B is presented sketchily at the medium-to-advanced level. Some of the details are relatively standard and may serve as a checklist or can be skipped altogether at first reading. Specific material begins with subsections III A6 and continues across subsection III B.

A. General outline for the polyad approximation

Consider the original classical dynamical system which represents vibrations of the molecule with K vibrational degrees of freedom.[5] In the most standard setup, coordinates Q in $\mathbb{R}^K$ describe small distortions of the equilibrium geometric configuration of the molecule (in the given electronic state) at $Q = 0$. The dynamics takes place on the phase space $T\mathbb{R}^K$ with dynamical variables (P,Q) and standard symplectic structure $dP \wedge dQ$. The energy is given by the vibrational Hamiltonian $H(Q,P)$ with an elliptic equilibrium at $Q = P = 0$.

1. Resonances and polyads

The origin of polyads is in the (near) *resonance*

$$k_1^{-1}\omega_1 \approx k_2^{-1}\omega_2 \approx \cdots \approx k_K^{-1}\omega_K \approx \omega_0$$

of the frequencies ω_i with $i = 1,\ldots,K$, of the linearization of this system at $P = Q = 0$, i.e., of the harmonic frequencies of the quadratic Hamiltonian

$$H_0(Q,P) \approx \omega_0 \mathcal{N}(Q,P),$$

[5]For a nonlinear s-atomic molecule, $K = 3s - 6$.

where

$$H_0(Q,P)=\frac{1}{2}\sum_i^K \omega_i\left(P_i^2+Q_i^2\right),\quad \text{and}$$

$$\mathcal{N}(Q,P)=\frac{1}{2}\sum_i^K k_i\left(P_i^2+Q_i^2\right)=\sum_i^K k_i N_i.$$

The polyad approximation is enforced by normalizing $H(Q,P)$ with respect to the flow $\varphi_{\mathcal{N}}^t$ of the Hamiltonian vector field $X_{\mathcal{N}}$ of the polyad integral $\mathcal{N}(Q,P)$. This involves a near-unity canonical transformation $(Q,P)\mapsto(q,p)$ and gives the *normal form* $\mathcal{H}(q,p)$ which depends on the dynamical variables (q,p) of the normalized system.

2. Reduction of polyad symmetry

The normalized system still has K degrees of freedom, but it now has a built-in strict $\mathbb{S}^1$ Lie symmetry which is given by $\varphi_{\mathcal{N}}^t$ and which acts on the phase space $T\mathbb{R}^K$ so that $\mathcal{H}(q,p)$ remains invariant. Note that because it is defined by a Hamiltonian flow [as opposed, for example, to an SO(2) rotation symmetry group acting on the configuration space], this symmetry is called *dynamical*; since it defines quantum polyads, it is called *polyadic*; since the resonance condition is not exact and higher orders in the initial $H(Q,P)$ are not invariant with respect to this symmetry, it is *approximate*. Reducing the polyadic symmetry, we eliminate the associated universal polyad degree of freedom. Technically, in the process of reduction, the polyad integral $\mathcal{N}(q,p)$ is replaced by its value $n\geqslant 0$ which becomes a *parameter*. In that way, we obtain *reduced* Hamiltonian $\mathcal{H}_n$ on the compact reduced phase space $\mathcal{P}_n$ of real dimension $2K-2$ called *polyad space*. Each point of $\mathcal{P}_n$ lifts to a circular orbit $\gamma_n\subset T\mathbb{R}^K$ of $\varphi_{\mathcal{N}}^t$, or an $\mathcal{N}$-orbit for brevity. $\mathcal{P}_n$ is generally a weighted projective space on which the symplectic structure can be defined only locally. So it is convenient to describe $\mathcal{P}_n$ and the reduced (or internal polyad) dynamics under $\mathcal{H}_n$ within an Euler-Poisson framework using a set of generators of the Poisson algebra of the reduced system.

3. Integrable approximation

The normal form $\mathcal{H}(q,p)$ and reduced Hamiltonian $\mathcal{H}_n$ are formal series in the parameter ε of the perturbations due to nonlinear terms. Except for the case $K=1$ of the diatomic molecule, this series is known to diverge eventually. Nevertheless—and there is the main practical value of the polyad approximation—truncated series $\mathcal{H}(q,p)$ and $\mathcal{H}_n$ can give a fair approximation to the original nonintegrable dynamics. Below we will always imply that $\mathcal{H}(q,p)$ and $\mathcal{H}_n$ are truncated. Because $\mathcal{H}(q,p)$ and $\mathcal{N}(q,p)$ Poisson commute, we call the approximation given by $\mathcal{H}(q,p)$ *integrable*. This does not mean, of course, that the normalized system is integrable, because the nonintegrability of the internal polyad dynamics with $K-1$ degrees of freedom is preserved.

4. Simple examples

Spectroscopists call Hamiltonians $\mathcal{H}(q,p)$ and $\mathcal{H}_n$ as *model* (because they rely on the assumption of a certain resonance condition and associated polyad symmetry $\mathbb{S}^1$) and *effective* (because all "nondiagonal" interactions between polyads are accounted for effectively and indirectly). To have a simple example, think of $K=2$. In that case, the space $\mathcal{P}_n$ is homeomorphic and, for the 1:1 resonance, diffeomorphic to a two-sphere $\mathbb{S}^2$, i.e., the $\mathbb{C}P^1$ space. The Poisson algebra of the reduced system is similar to the so(3) algebra of the Euler top. The polyad approximation is completely integrable. In the molecular literature (on such molecules as H_2O, O_3 and others) [32], the particular case of the two modes in 1:1 resonance has been traditionally called the polyad approximation [33,34]. It was used in systems with other resonances [35,36], such as 2:1:1 in CO_2 and polyads of acetylene [37–39]. We further extend and develop this concept mathematically. A more substantial review of the relevant work can be found in Refs. [3,20,40].

5. Quantization and quantum-classical correspondence

From the quantum mechanical point of view, the main advantage of the polyad approximation is that it results in the finite set of basis functions or, more correctly, in working on finite-dimensional subspaces of the Hilbert space. Those of us who think quantum-mechanically see this as block-factorization of the matrix of the original quantum Hamiltonian $\hat{H}(Q,P)$ resulting from the quantum analog of the Lie transform normalization techniques called Van-Vleck transformation (see, for example, calculations for methane in Ref. [14]). From the semiclassical perspective, that we take in this work, this is a consequence of the compactness of reduced phase spaces $\mathcal{P}_n$.

In comparison to its quantum counterparts [14], classical normalization reproduces only principal terms of quantum commutators. So, strictly speaking, quantization and polyad normalization do not commute. However, for many purposes, including ours, corrections arising from the nonprincipal terms can be neglected. Furthermore, for any spectroscopic purpose, parameters of $\mathcal{H}_n$ have to be adjusted to reproduce experimental data satisfactorily, and these adjustments are comparable to the quantum corrections we neglect.

The normalized system with Hamiltonian $\mathcal{H}(q,p)$ can be quantized straightforwardly by replacing (q,p) for $(q,-i\hbar\partial/\partial p)$. The eigenfunctions of the resulting quantum Hamiltonian $\hat{\mathcal{H}}$ for a given polyad n can be constructed using oscillator basis functions $|n_1\rangle|n_2\rangle\cdots|n_K\rangle$ that satisfy

$$\sum_{i=1}^K k_i n_i = n.$$

For a given $n\gg 1$, the polyad Hilbert space is spanned by approximately

$$\frac{n^{K-1}}{(k_1k_2\cdots k_K)(K-1)!}+O(n^{K-2})$$

functions [41]; the exact number is given by the n-th degree coefficient of the Taylor expanded generating function

$$g(\lambda)=\prod_{i=1}^K(1-\lambda^{k_i})^{-1}.$$

The eigenspectrum of $\hat{\mathcal{H}}$ approximates the energies of the system. The reduced system with Hamiltonian $\mathcal{H}_n$ can be quantized by replacing generators of its Poisson algebra for appropriate quantum operators [42–44]. In the simple 1:1 example, this gives the standard algebra of angular momentum operators. And, of course, for $K \leqslant 2$ we can use the EBK quantization principle.

6. *Relative equilibria and internal polyad structure*

When the linearized system has degeneracies due to symmetries and resonances, the normal modes reflect little if any dynamics of the system. We should use the *nonlinear normal modes* [16–19] instead. These are families of short-period periodic orbits that survive breaking the degeneracy by a system-specific nonlinear perturbation [45,46]; their number is typically *larger* than K. Nonlinear normal modes can be approximated by lifting nondegenerated stationary points of $\mathcal{H}_n$ on $\mathcal{P}_n$ back to the original phase space $T\mathbb{R}^K$ where they become $\mathcal{N}$ orbits of period $\approx 2\pi/\omega_0$. So, within the polyad approximation, nonlinear normal modes become *relative equilibria*[6] (RE) of the system.

The importance of RE to the analysis of polyads has been demonstrated repeatedly (see Refs. [3,19,20] and references therein). Because RE make up the "skeleton" of a polyad, the study of any polyad system begins with finding and describing its RE for different values n of the polyad integral $\mathcal{N}$. In other words, we consider one-parameter families of RE. As n increases, this includes uncovering bifurcations, which may, in particular, create new additional RE. The most known example is the creation of *local modes* in H_2O, O_3, and other molecules. Results of the RE analysis can be represented using an energy-momentum diagram (otherwise known as bifurcation diagram) where energies of $\mathcal{H}_n$ at different RE are displayed as functions of n. For $K = 2$ such diagram provides a very detailed characterization of polyads; for large $K > 2$, interpreting the RE structure of the polyad becomes more challenging.

B. Classical description of polyads of methane

The vibrational Hamiltonian of methane is a function of $K = 9$ vibrational normal mode coordinates q and corresponding conjugate momenta p. Our choice of coordinates, numbering of hydrogen atoms, and principal symmetry operations that generate cubic groups are illustrated in Fig. 2. The usual spectroscopic notation is based on the normal mode index $1 \ldots 4$, the irreducible representation Γ and its row σ, according to which the particular coordinate transforms. We will use complex oscillator variables

$$z = q - ip, \quad \bar{z} = q + ip,$$

which are direct analogs of quantum creation-annihilation operators $\sqrt{2}a$ and $\sqrt{2}a^\dagger$ and the following shorthand notation

z	Mode	Γ	σ	k	Type
z_1	ν_1	A_1		2	Stretching
z_2	ν_2	E	a	1	Bending
z_3			b	1	
z_4	ν_3	F_2	x	2	Stretching
z_5			y	2	
z_6			z	2	
z_7	ν_4	F_2	x	1	Bending
z_8			y	1	
z_9			z	1	

where k indicates the factor in the resonance condition (1).

1. *Normalized Hamiltonian $\mathcal{H}$ and reduced Hamiltonian $\mathcal{H}_n$*

In the presence of resonance (1), the system can be normalized with regard to the periodic flow of the nine-dimensional harmonic oscillator system with Hamiltonian

$$\mathcal{N}(z) = z_1\bar{z}_1 + \frac{1}{2}\sum_{i=2}^{3} z_i\bar{z}_i + \sum_{i=4}^{6} z_i\bar{z}_i + \frac{1}{2}\sum_{i=7}^{9} z_i\bar{z}_i. \quad (3)$$

Each $\mathcal{N}$-orbit γ_n is a specific simultaneous rotation of symplectic planes $(z_i,\bar{z}_i)$, $i = 1 \ldots 9$. Starting γ_n at time $t = 0$ and point $z = (z_1, z_2, \ldots, z_9)$, where $\mathcal{N}(z) = n$, we have

$$\gamma_n : z \mapsto (z_1\theta^2, (z_2,z_3)\theta, (z_4,z_5,z_6)\theta^2, (z_7,z_8,z_9)\theta),$$

where $\theta = e^{it}$, $\bar{\theta} = e^{-it}$, and $t \in [0, 2\pi]$.

In order to remain invariant along γ_n, the monomials in the normal form $\mathcal{H}(z,\bar{z})$ should be of certain specific form, e.g.,

$$z_1\bar{z}_2^2, \quad z_4\bar{z}_2\bar{z}_7, \quad \text{etc};$$

they should include such products of z and $\bar{z}$ for which the θ factors vanish. Further restrictions on the allowed terms in $\mathcal{H}(z,\bar{z})$ are imposed by the $T_d \times \mathcal{T}$ symmetry [3,4].

There are two ways of arriving at $\mathcal{H}$: (i) Similarly to Ref. [14], one can take the original vibrational Hamiltonian $H(Q,P)$ that includes a potential surface $V(Q)$ and normalize it. (ii) We can take a shortcut and start with the well-developed spectroscopic phenomenological rovibrational Hamiltonian $\mathcal{H}$ of the Dijon group (see Table II, Refs. [7,8] and references therein). Because $V(Q)$ of methane is not sufficiently well determined, the second method gives currently more accurate predictions for higher polyads. Furthermore, our purpose is the subsequent analysis based on $\mathcal{H}$ and the method by which $\mathcal{H}$ is obtained is not important, so we followed the second path. The spectroscopic Hamiltonian $\mathcal{H}$ in Table II is already in normal form but its terms are defined implicitly using the Wigner-Eckart theorem and various coefficients [4]. Explicit expressions for the Hamiltonian used in Refs. [7,8], such as the ones in Ref. [20], can be obtained by a careful analysis of definitions in Ref. [4]. Thus we get the quadratic part

$$\mathcal{H}^0 = \frac{\omega_1}{2}z_1\bar{z}_1 + \frac{\omega_2}{2}\sum_{i=2}^{3} z_i\bar{z}_i + \frac{\omega_3}{2}\sum_{i=4}^{6} z_i\bar{z}_i + \frac{\omega_4}{2}\sum_{i=7}^{9} z_i\bar{z}_i,$$

[6]For an introduction to relative equilibria and definitions, see Appendix 5C of Ref. [47] and Chap. 3.3 of Ref. [48]; for a more specific discussion, see Ref. [49].

TABLE II. Terms in the vibrational Hamiltonian of methane used by Boudon *et al.* [7]: d is total degree in vibrational variables, Δ is the number of bending-size quanta exchanged by the term, $\Gamma'_{\pm}$ and $\Gamma''_{\pm}$ and $\Gamma_{\pm}=\Gamma$ are intermediate irreducible representations of the T_d point group used in the tensorial definition by Champion *et al.* and Wenger and Champion [4,5]; monomials of O(3) type K and degree $d_i \geqslant K$ are denoted as $d_i K \Gamma_i$, indices of creation-annihilation variables $a^{\dagger}$ and a correspond to normal modes.

Parameter	Value cm^{-1}	d	(Δ)	Γ	Γ'_+	Γ''_+	$a_1^{\dagger}$	$a_2^{\dagger}$	$a_3^{\dagger}$	$a_4^{\dagger}$	Γ'_-	Γ''_-	a_1	a_2	a_3	a_4
ω_1	2882.40935	2	(2)	A_1	A_1	A_1	$10A_1$				A_1	A_1	$10A_1$			
ω_2	1533.33258	2	(1)	E	E	E		$11E$			E	E		$11E$		
ω_3	2998.45069	2	(2)	F_2	A_1	F_2			$11F_2$		A_1	F_2			$11F_2$	
ω_4	1310.76161	2	(1)	F_2	A_1	A_1				$11F_2$	A_1	A_1				$11F_2$
t_{344}	−52.17645	3	(2)	F_2	A_1	F_2			$11F_2$		A_1	A_1				$22F_2$
t_{324}	−49.84192	3	(2)	F_2	A_1	F_2			$11F_2$		E	E		$11E$		$11F_2$
t_{144}	100.38526	3	(2)	A_1	A_1	A_1	$10A_1$				A_1	A_1				$20A_1$
t_{122}	7.31404	3	(2)	A_1	A_1	A_1	$10A_1$				A_1	A_1		$20A_1$		
t_{4444}	3.09905	4	(2)	E	A_1	A_1				$22E$	A_1	A_1				$22E$
t_{2444}	0.51881	4	(2)	F_2	E	E		$11E$		$11F_2$	A_1	A_1				$22F_2$
t_{2424}	1.98394	4	(2)	F_1	E	E		$11E$		$11F_2$	E	E		$11E$		$11F_2$
t_{2244}^{E}	−1.35085	4	(2)	E	E	E		$22E$			A_1	A_1				$22E$
$t_{2244}^{A_1}$	−10.69933	4	(2)	A_1	A_1	A_1		$20A_1$			A_1	A_1				$20A_1$
t_{2222}^{E}	−1.52673	4	(2)	E	E	E		$22E$			E	E		$22E$		
$t_{2222}^{A_1}$	−3.43159	4	(2)	A_1	A_1	A_1		$20A_1$			A_1	A_1		$20A_1$		
$t_{3434}^{F_2}$	−11.24401	4	(3)	F_2	A_1	F_2			$11F_2$	$11F_2$	A_1	F_2			$11F_2$	$11F_2$
$t_{3434}^{F_1}$	−19.94961	4	(3)	F_1	A_1	F_2			$11F_2$	$11F_2$	A_1	F_2			$11F_2$	$11F_2$
t_{3434}^{E}	−19.06810	4	(3)	E	A_1	F_2			$11F_2$	$11F_2$	A_1	F_2			$11F_2$	$11F_2$
$t_{3434}^{A_1}$	−33.08916	4	(3)	A_1	A_1	F_2			$11F_2$	$11F_2$	A_1	F_2			$11F_2$	$11F_2$
$t_{2334}^{F_2}$	0.21457	4	(3)	F_2	E	F_2		$11E$	$11F_2$		A_1	F_2			$11F_2$	$11F_2$
$t_{2334}^{F_1}$	10.95242	4	(3)	F_1	E	F_1		$11E$	$11F_2$		A_1	F_2			$11F_2$	$11F_2$
$t_{2323}^{F_2}$	−22.58362	4	(3)	F_2	E	F_2		$11E$	$11F_2$		E	F_2		$11E$	$11F_2$	
$t_{2323}^{F_1}$	−15.55456	4	(3)	F_1	E	F_1		$11E$	$11F_2$		E	F_1		$11E$	$11F_2$	
t_{1434}	14.49813	4	(3)	F_2	A_1	A_1	$10A_1$			$11F_2$	A_1	F_2			$11F_2$	$11F_2$
t_{1423}	34.60149	4	(3)	F_2	A_1	A_1	$10A_1$			$11F_2$	E	F_2		$11E$	$11F_2$	
t_{1414}	−21.44273	4	(3)	F_2	A_1	A_1	$10A_1$			$11F_2$	A_1	A_1	$10A_1$			$11F_2$
t_{1234}	−11.09301	4	(3)	E	E	E	$10A_1$	$11E$			A_1	F_2			$11F_2$	$11F_2$
t_{1212}	−9.67220	4	(3)	E	E	E	$10A_1$	$11E$			E	E	$10A_1$	$11E$		
$t_{3333}^{F_2}$	−14.26190	4	(4)	F_2	A_1	F_2			$22F_2$		A_1	F_2			$22F_2$	
t_{3333}^{E}	10.39318	4	(4)	E	A_1	E			$22E$		A_1	E			$22E$	
$t_{3333}^{A_1}$	−150.42460	4	(4)	A_1	A_1	A_1			$20A_1$		A_1	A_1			$20A_1$	
t_{1333}	−6.31920	4	(4)	F_2	A_1	F_2	$10A_1$		$11F_2$		A_1	F_2			$22F_2$	
t_{1313}	−98.79672	4	(4)	F_2	A_1	F_2	$10A_1$		$11F_2$		A_1	F_2	$10A_1$		$11F_2$	
t_{1113}	−3.15814	4	(4)	A_1	A_1	A_1	$20A_1$				A_1	A_1			$20A_1$	
t_{1111}	−30.25501	4	(4)	A_1	A_1	A_1	$20A_1$				A_1	A_1	$20A_1$			

and the cubic part

$$\begin{aligned}\mathcal{H}^1 = &-\frac{t_{144}}{4\sqrt{3}} z_1\left(\bar{z}_7^2+\bar{z}_8^2+\bar{z}_9^2\right) - \frac{t_{122}}{4\sqrt{2}} z_1\left(\bar{z}_2^2+\bar{z}_3^2\right)\\ &+\frac{t_{344}}{2\sqrt{2}}\left(z_4\bar{z}_8\bar{z}_9+z_5\bar{z}_7\bar{z}_9+z_6\bar{z}_7\bar{z}_8\right)\\ &+\frac{t_{324}}{4\sqrt{2}} z_2\left(\bar{z}_4 z_7+\bar{z}_5 z_8-2\bar{z}_6 z_9\right)\\ &-\frac{t_{324}}{4\sqrt{2}}\sqrt{3} z_3\left(\bar{z}_4 z_7-\bar{z}_5 z_8\right)+\text{c.c.}\end{aligned}$$

In the present work, we went up to the quartic terms; their expressions are lengthy and we do not provide them here.

To reduce the normalized system with Hamiltonian $\mathcal{H}(z,\bar{z})$ we first construct and describe the reduced phase space $\mathcal{P}_n$ as a (possibly singular) Poisson manifold using a certain number of polynomial generators of the Poisson algebra of the reduced system. Then we rewrite $\mathcal{H}(z,\bar{z})$ so that it becomes a function $\mathcal{H}_n$ of the above generators, in other words, a function on $\mathcal{P}_n$, and parameter n. For polyads with $K-1=8$ internal degrees of freedom, the latter operation is, however, hardly advantageous because the generator basis is large and is complicated by sygyzies. So instead we will use appropriate $\mathbb{C}^8$ *charts* of $\mathcal{P}_n$ and work essentially with $\mathcal{H}(z,\bar{z})$ projected in the charts. See Refs. [3,20,50] for key technical aspects and the following section.

2. *Projective decomposition of the reduced phase space $\mathcal{P}_n$*

Reduced Hamiltonian $\mathcal{H}_n$ is a function on the polyad space $\mathcal{P}_n$ of real dimension 8×2. Points of $\mathcal{P}_n$ can be described using complex variables z by the method outlined in Ref. [20]. Following [20], we *decompose* the large polyad space in terms of several polyad subspaces or *polyad projections*. Each projection is itself a polyad space of a smaller system. Thus the ν_2 projection is a polyad space of isolated ν_2 polyads, i.e., of a system of two oscillators in 1:1 resonance (with a specific C_{3v} symmetric perturbation similar to that in the Hénon–Heiles potential). It is, therefore, a $\mathbb{C}P^1 \sim \mathbb{S}^2$ [3]. Similarly, both the ν_3 and the ν_4 projections have $\mathbb{C}P^2$ topology. We combine projections by introducing *mixing coordinates* for amplitude $\eta \in [0,1]$ and phase and $\phi \in [0,2\pi)$. Specifically, we write

$$z = \sqrt{n} \begin{pmatrix} \sqrt{\eta_1}\exp(i\phi_1)\zeta_1 \\ \sqrt{2\eta_2}\exp(i\phi_2)(\zeta_2,\zeta_3) \\ \sqrt{1-\eta_1-\eta_2-\eta_4}(\zeta_4,\zeta_5,\zeta_6) \\ \sqrt{2\eta_4}\exp(i\phi_4)(\zeta_7,\zeta_8,\zeta_9) \end{pmatrix}, \tag{4}$$

where $\zeta_1 \equiv 1$ for ν_1, and unimodular vectors (ζ_2,ζ_3), $(\zeta_4,\zeta_5,\zeta_6)$, and $(\zeta_7,\zeta_8,\zeta_9)$ define points on the respective ν_2, ν_3, and ν_4 polyad projections. Note that the space described by coordinates (ζ,ϕ) is itself a projective space. Substituting in (3), we can verify that $\mathcal{N}(z) = n$ for any z defined by (4). The simplest two-mode mixing case of stretching modes ν_1 and ν_3 ($K = 4$) which required one pair of mixing coordinates (η_1,ϕ_1) was studied in Ref. [20]. In the general case of Eq. (4), we should use six such coordinates to mix all four normal modes. Also note that Eq. (4) implies that $\eta_1 + \eta_2 + \eta_4 < 1$, i.e., that the ν_3 contribution is nonzero. Furthermore, this form is most efficient when $\eta_1 + \eta_2 + \eta_4 \ll 1$. Such representation is called a ν_3 chart of $\mathcal{P}_n$.

3. *Relative equilibria (RE)*

In our case, a general search for RE is a formidable task that requires finding stationary points of function $\mathcal{H}_n$ (equilibria) on a curved compact space $\mathcal{P}_n$ of real dimension 16. We should first exploit fully the symmetry group $T_d \times \mathcal{T}$ of our system. Specifically, $T_d \times \mathcal{T}$ acts on $\mathcal{P}_n$ in such a way that $\mathcal{P}_n$ becomes stratified in various low-dimensional subspaces that are invariant with respect to subgroups $G \subseteq T_d \times \mathcal{T}$, called *stabilizers* or *isotropy groups*. For a G-isotropic subspace, all nonvanishing components of $\nabla\mathcal{H}_n$ should be tangent to it, and if G is symplectic, the dynamics may be restricted to it as well. Obviously, the search for possible particular solutions becomes easier with decreasing dimension.

We can argue using the principles of Morse theory [51] that among all RE, there must be a number of RE that are invariant with regard to different stabilizers $G \subseteq T_d \times \mathcal{T}$. In the simple "minimal" cases, in particular at low n, our $\mathcal{H}_n$ may have only symmetric stationary points with sufficiently large stabilizers G whose existence is caused primarily by the action of the symmetry group $T_d \times \mathcal{T}$ and the topology of $\mathcal{P}_n$ [51]. These RE are much easier to find as stationary points of $\mathcal{H}_n$ on $\mathcal{P}_n$ (because several equations in $\nabla\mathcal{H}_n = 0$ are satisfied autmatically due to symmetry). They correspond to points of $\mathcal{P}_n$ that belong to specific nongeneric orbits of the $T_d \times \mathcal{T}$ action. The set of all orbits of the same type form a *stratum*. The topology of the system of strata and, specifically, the presence of low-dimensional isolated components within a stratum and within this system is of prime importance here. In the simplest case, we may find isolated points that represent *critical* orbits. Points on such orbits are *necessarily* G-invariant stationary points of $\mathcal{H}_n$ [51].

TABLE III. Representatives of isolated fixed points of the $T_d \times \mathcal{T}$ group action on the ν_3 and ν_4 polyad subspaces $\mathbb{C}P^2$, the ν_2 subspace $\mathbb{C}P^1$, and the rotational sphere $\mathbb{S}^2$ [3]. For each representative, we indicate the class of conjugated subgroups of $T_d \times \mathcal{T}$ of its stabilizer and give in parentheses the number of equivalent points with stabilizer in the same class.

Stabilizer		$\mathbb{C}P^1$		$\mathbb{C}P^2$			$\mathbb{S}^2$		
		ζ_2	ζ_3	$\zeta_{4,7}$	$\zeta_{5,8}$	$\zeta_{6,9}$	j_1	j_2	j_3
$D_{2d} \times \mathcal{T}$	(3)	1	0	1	0	0	1	0	0
$C_{3v} \times \mathcal{T}$	(4)	b	ib	a	a	a	a	a	a
$C_{2v} \times \mathcal{T}$	(6)	1	0	b	b	0	b	b	0
$S_4 \wedge \mathcal{T}_2$	(6)	1	0	b	ib	0	1	0	0
$C_3 \wedge \mathcal{T}_s$	(8)	b	ib	a	$\chi^2 a$	χa	a	a	a

Here $a = 1/\sqrt{3}$, $b = 1/\sqrt{2}$, $\chi = e^{i\pi/3}$.

We turn to studying how $T_d \times \mathcal{T}$ acts on our 16-dimensional $\mathcal{P}_n$. The dimension of $\mathcal{P}_n$ is too high for critical orbits to occur; instead, we have "small" isolated G-invariant subspaces of $\mathcal{P}_n$.[7] We like to find G-invariant subspaces $\mathcal{P}_n^G \subset \mathcal{P}_n$ with smallest possible dimension. Such subspaces will be called *minimal fixed spaces* of the $T_d \times \mathcal{T}$ action on $\mathcal{P}_n$.

In order to find minimal G-invariant subspaces $\mathcal{P}_n^G$, we take advantage of our decomposition of $\mathcal{P}_n$ in Eq. (4). We study the action of $T_d \times \mathcal{T}$ on each of the polyad projections of $\mathcal{P}_n$, namely the $\mathbb{C}P^1 \sim \mathbb{S}^2$ space of isolated ν_2 polyads and the $\mathbb{C}P^2$ space of isolated ν_3 polyads. On all these spaces, the action of $T_d \times \mathcal{T}$ has critical orbits [3,50]. So it follows that $\mathcal{P}_n^G$ *is minimal if in each projection it is represented by a fixed point on the critical orbit of the $T_d \times \mathcal{T}$ action on this projection.* When all modes are present (i.e., if neither of the amplitude mixing coordinates η is 0), we can deduce from Eq. (4) that minimal fixed spaces are 2:1:2:1 weighted projective spaces of real dimension 6. Fixed points in the $\mathbb{C}P$ projections were determined in Ref. [3,50] for all possible stabilizers G. We list them in Table III. We also give the corresponding fixed points (j_1,j_2,j_3) on the rotational sphere $\mathbb{S}^2$ to allow extending the analysis to rotation-vibration Hamiltonians $\mathcal{H}(z,\bar{z},j)$, but for now we assume no rotation ($j = 0$) for simplicity.

Using information in Table III requires basic understanding of the $T_d \times \mathcal{T}$ action on projective spaces. The idea is to substitute coordinates ζ in Eq. (4) for the ones in this table and allow for mixing coordinates (η,ϕ) to vary. However, this will not always preserve the isotropy because $G \subseteq T_d \times \mathcal{T}$

[7] In a more rigorous context, we should be more explicit in describing a G-invariant subspace. In addition to points with stabilizer G, it may (and usually does) contain points with higher stabilizers $G' \supset G$. Obviously, such subspace corresponds to a union of certain isolated components of several nongeneric strata. This also means that $T_d \times \mathcal{T} \supseteq G' \supset G$ acts nontrivially on it, i.e., the image of $T_d \times \mathcal{T}$ is not 1. For examples of such subspaces, see subsections III C1 and III C2.

may act nontrivially on the phase-mixing coordinates ϕ and produce nontrivial automorphisms $\mathcal{P}_n^G \hookleftarrow$. As a result, the actual stabilizers $\tilde{G} \subseteq G$ of points of $\mathcal{P}_n^G$ may be lower and $\mathcal{P}_n^G$ may contain lower dimensional strata of points with nontrivial isotropy. So, in general, G refers to the symmetry of the projections of $\mathcal{P}_n^G$ and not to the actual stabilizer of its points. For this reason we will call G *projected stabilizer*.

For example [20], from Eq. (4) with $\eta_2 = \eta_4 = 0$ we can see that $\mathcal{T} : z \mapsto \bar{z}$ acts on purely stretching subspaces as $\phi_1 \mapsto -\phi_1$. In fact [20], purely stretching symmetry preserving normal mode mixing is only allowed for the two topmost stabilizers in Table III which we will call for brevity D_{2d} and C_{3v}. Of course, mixing is always possible for generic RE that appear eventually with growing n as the dynamics becomes increasingly irregular, but mixing possibilities at low n seem to be quite limited.

This remarkable result is little known, and its full value remains to be uncovered. Because we are interested primarily in mixing, we focus in subsection III C below on RE of these two types. Other symmetric RE, though nonlinear in nature, are of nonmixed normal mode content and are likely (as in the case studied in Ref. [20]) to be unstable.

C. Symmetric stretching relative equilibria

Now we can find RE as symmetric stationary points of $\mathcal{H}_n$. For all possible stablizers $G \subseteq T_d \times \mathcal{T}$, we restrict $\mathcal{H}_n$ on minimal fixed spaces $\mathcal{P}_n^G$ and search for stationary points of the restricted function $\mathcal{H}_n\big|\mathcal{P}_n^G : \mathcal{P}_n^G \to \mathbb{R}$. The search can be further simplified by taking the stratification of $\mathcal{P}_n^G$ into account. Note also that polar coordinates (η,ϕ) do not reflect correctly the geometry of $\mathcal{P}_n^G$ and should be used with usual precautions at "poles" $\eta = 0$ and $\eta = 1$. Ideally, one should analyze the whole family of vibrational polyad RE of methane (and extend them to rotational-vibrational RE). This, however, is not immediately feasible here. Our approach is relatively new and we like to develop it more fully on a small number of examples. So we restrict the analysis to a few potentially most important RE.

We turn here to stabilizers C_{3v} and D_{2d} because they allow normal mode mixing and because such highly symmetric RE are more likely to remain elliptic. Additionally, we will neglect bending contributions, assuming $\eta_2 = \eta_4 = 0$. This has two aspects. One of the C_{3v} RE is smoothly related [20] to what spectroscopists call local mode [10,12,28–31]. Local modes are well pronounced in certain molecules and we like to clarify the situation in methane. At the same time, we also like to minimize the theory required for understanding our particular experimental results. Because of the 2:1 stretching-to-bending frequency ratio, absorbing stretching vibrational quanta is the "shortest" way to reach highly excited polyads. In the Taylor series for the effective polyad transition moment μ_{eff} (see Sec. IV), the lowest degree terms describing the $P_0 \to P_n$ transition are of maximal degree $\approx n/2$ in stretching variables (z_1,z_4,z_5,z_6). Intensity depends both on the coefficient in the μ_{eff} series and the upper state wave function. So it makes sense to investigate whether absorption can be channeled in a predominantly stretching localized vibration.

1. The C_{3v} RE

Substituting subsequently z in Eq. (4) and ζ for stabilizer $C_{3v} \times \mathcal{T}$ in Table III into $\mathcal{H}(z) = \mathcal{H}^0(z) + \mathcal{H}^1(z) + \mathcal{H}^2(z)$ described in subsection III B, we obtain a function $\mathcal{H}_n^{C_{3v}}(\eta,\phi)$, where in the ν_3 chart we have $\eta = (\eta_1,\eta_2,\eta_4)$ and similarly $\phi = (\phi_1,\phi_2,\phi_4)$. $\mathcal{H}_n^{C_{3v}}(\eta,\phi)$ lives on the mixing space of real dimension 6. Fixing $\eta \equiv (\eta_1,0,0)$, we project $\mathcal{H}_n^{C_{3v}}(\eta,\phi)$ on an $\mathbb{S}^2$ subspace with cylindrical coordinates (η_1,ϕ_1). This is the simplest mixing space [20]. Points of this space represent different phase and amplitude combinations of the two stretching modes ν_1 and ν_3 with projected stabilizer $C_{3v} \times \mathcal{T}$. The coupling space $\mathbb{S}^2$ is cut into two halves by the above mentioned action of $\mathcal{T}$. The respective reflection plane $\{\phi_1 = 0,\pi\}$ intersects $\mathbb{S}^2$ on a circle $\mathbb{S}^1$ of $C_{3v} \times \mathcal{T}$-invariant points with one exceptional $T_d \times \mathcal{T}$-invariant fixed point ν_1. All other points have isotropy C_{3v}. Defining longitude and latitude angles $\theta \in [0,\pi]$ and $\phi \in [0,2\pi)$ so that

$$\eta_1 = (1 + \cos\theta)/2, \quad \text{and} \quad \phi_1 = \phi,$$

and using the values of parameters in Table II, we obtain

$$\mathcal{H}_n^{C_{3v}} = \mathcal{H}' + \mathcal{H}'' - 0.45605\, n^2 \sin\theta(1 - \cos\theta)\cos\phi + (3.47924\cos^2\theta + 1.83715\cos\theta - 9.0983)\, n^2,$$

where

$$\mathcal{H}' = (48.1679 - 29.0103\cos\theta)\, n,$$
$$\mathcal{H}'' = (0.22792\sin^2\theta\cos^2\phi)\, n^2.$$

This function is depicted in Fig. 7 for $n = 8$. We can see that it has a maximum at the north pole (pure ν_1), a similar hight maximum near the south pole, and a shallow minimum-saddle pair in the ravine at $\eta_1 \approx 1/2$ (near 50% mixing). All these critical points on $\mathbb{S}^2$ correspond to different stretching C_{3v} RE. Finding them has been described in more detail in Ref. [20].

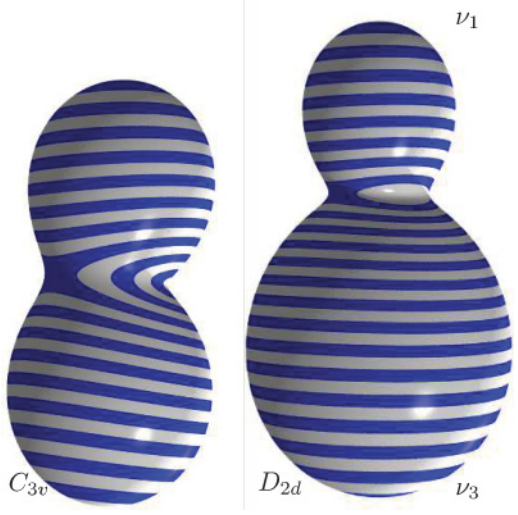

FIG. 7. (Color online) Coupling surfaces of stretching (ν_1,ν_3) relative equilibria of methane with isotropy C_{3v} (left) and D_{2d} (right) for polyad P_8. The surfaces are stripe painted at fixed equidistant energy intervals; pure ν_1 and ν_3 are at $\phi = 0$ (north) and $\phi = \pi$ (south) poles. The D_{2d} surface has a vertical symmetry axis C_2 while the C_{3v} one does not; the latter has no stationary point exactly at $\phi = \pi$.

We notice that the Hamiltonian $\mathcal{H}_n^{C_{3v}}$ is $\mathcal{T}$ invariant and is therefore symmetric with respect to the reflections $\phi \mapsto -\phi$.

All stationary points that we have found lie on the $\mathcal{T}$ circle. The *fixed* point at the north pole represents 100% pure ν_1 mode. The point near the south pole is not fixed; it can move on $\mathbb{S}^1$, but it does it only slightly, and the respective RE remains very close to pure ν_3. This differs from the local mode scenario [20] where this RE evolves smoothly into the local mode with ≈30% ν_1 content. The two other stationary points represent additional strongly mixed stretching RE; they appear as a result of a bifurcation of the ν_1 RE; see subsection III C3.

For the purposes of our later analysis, it is instructive to look more closely at the near south pole RE. Since it is almost pure ν_3, it can be characterized sufficiently well by the invariant variables

k	$n_{3,k}$	$s_{3,k}$	$t_{3,k}$
1	$(z_4\bar{z}_4)/2$	$(z_5\bar{z}_6+z_6\bar{z}_5)/2$	$(z_5\bar{z}_6+z_6\bar{z}_5)i/2$
2	$(z_5\bar{z}_5)/2$	$(z_4\bar{z}_6+z_6\bar{z}_4)/2$	$(z_6\bar{z}_4+z_4\bar{z}_6)i/2$
3	$(z_6\bar{z}_6)/2$	$(z_4\bar{z}_5+z_5\bar{z}_5)/2$	$(z_4\bar{z}_5+z_5\bar{z}_5)i/2$

describing the internal polyad dynamics on the ν_3 subspace $\mathbb{C}P^2 \subset \mathcal{P}_n$; cf. Table 21 and 31 of Ref. [3]. Notice that vector $t_3 = (t_{3,1}, t_{3,2}, t_{3,3})$ represents the angular momentum induced by the ν_3 vibrations. Using Eq. (4) and the $C_{3v} \times \mathcal{T}$ entry in Table III, we obtain that $n_{3,k} \approx n/6$, $s_{3,k} \approx n/3$, and $t_3 = 0$. So it follows that quantum states localized near such RE should have very low (in comparison to the polyad number n) vibrational angular momentum.

2. The D_{2d} RE

Choosing the $D_{2d} \times \mathcal{T}$ entry in Table III and following the same approach as in the previous section, we obtain

$$\mathcal{H}_n^{D_{2d}} = \mathcal{H}' + \mathcal{H}'' + (3.99289\cos\theta^2 + 0.80985\cos\theta - 8.5846)n^2,$$

which is simpler than $\mathcal{H}_n^{C_{3v}}$. The reason is that the image of $D_{2d} \times \mathcal{T}$ acting on the D_{2d} coupling sphere $\mathbb{S}^2$ is an abstract symmetry group $D_2 = \mathbb{Z}_2 \times \mathcal{T}$, where the additional $\mathbb{Z}_2$ corresponds to the C_2 rotations about axes orthogonal to the S_4 axis and acts as $\phi \mapsto \phi + \pi$. This produces on $\mathbb{S}^2$ the spatial group C_{2v} with reflections in planes $\phi = 0, \pi$ and $\phi = \pm\pi/2$ and C_2 rotations about axis $\nu_1\nu_3$, under which the Hamiltonian $\mathcal{H}_n^{D_{2d}}$ is invariant. We depicted $\mathcal{H}_n^{D_{2d}}$ with $n = 8$ in Fig. 7 (right). Its stationary points lie on the symmetry strata: at the poles and in the planes. Both poles (on the rotation axis) are fixed points, they represent 100% pure ν_1 and ν_3. Points in the planes come in pairs and can move (pairwise) in one dimension when n is changed; they are created in the bifurcations of the ν_1 RE described in subsection III C3.

3. Bifurcations involving the C_{3v} and D_{2d} RE

We follow briefly the modifications that the stretching C_{3v} and D_{2d} RE families undergo with growing value $n + 6\frac{1}{2} > 0$ of the classical polyad integral[8] $\mathcal{N}$. In this context,

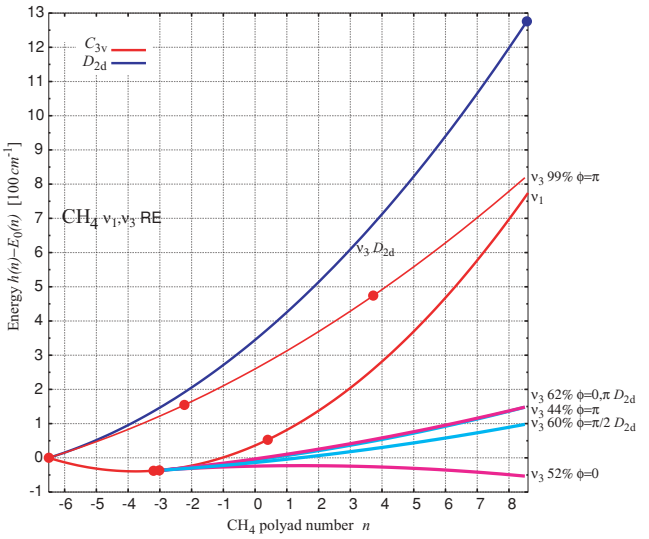

FIG. 8. (Color online) Energy of stretching (ν_1, ν_3) relative equilibria of methane as a function of polyad quantum number n. Circles mark bifurcations. Negative values of n correspond to classically allowed values $n + 6\frac{1}{2}$ of the polyad integral $\mathcal{N} \geqslant 0$.

Fig. 8 showing energies of stretching RE versus n serves as a bifurcation diagram. We notice first the characteristic qualitative deformation resulting from a series of closely succeeding bifurcations of the ν_1 RE near $\mathcal{N} \approx 3$. Like the local-mode-creating bifurcation in simpler systems (H_2O, SiH_4), this event takes place at very small $\mathcal{N}$, below the energy of the ground state, as a result of strong coupling between ν_1 and ν_3.

The smallest possible number of stationary points that a Morse function $\mathcal{H}_n^{\Gamma}$ can have on $\mathbb{S}^2$ is two, a minimum and a maximum. When $\mathcal{N} < 3$, both C_{3v} and D_{2d} coupling functions are of this simplest kind, with minimum at ν_1 and maximum at ν_3. We can say that the system is essentially uncoupled. Since the number of different C_{3v} and D_{2d} stabilizers is 4 and 3, respectively, the total number of stretching RE with these projected stabilizers is 8. (Think of four C_{3v} and three D_{2d} coupling spheres $\mathbb{S}^2$ all sharing their ν_1 poles; see Refs. [3,16,17] for details on counting the total number of nonlinear normal modes of methane.)

The first bifurcation occurs on the D_{2d} sphere at $\mathcal{N} \approx 3.298$. It is a pitchfork bifurcation with broken symmetry of order 2. The ν_1 RE goes unstable (on this sphere) and a pair of new stable D_{2d} RE with with $\phi = \pm\pi/2$ are emanated. As n increases, the pair descends south and takes more ν_3 content. Next we have a saddle-node bifurcation that takes place on the $\phi = 0$ semicircle of the C_{3v} sphere very close to the minimum at the ν_1 pole. It creates a new minimum which moves away from the pole (thus gaining ν_3 content) and a saddle that moves toward the pole. What happens can be best observed projecting the coupling sphere in the $\mathbb{R}^2$ plane tangent at the ν_1 pole with coordinates

$$(x, y) = \tfrac{1}{2}\sin\theta(\cos\phi, \sin\phi),$$

such that

$$\cos\theta = \sqrt{1 - 4(x^2 - y^2)}.$$

[8]The difference $\mathcal{N} - n$ is given by Eq. (2) with $n_1 = \frac{1}{2}$, $n_2 = 1$ and $n_3 = n_4 = \frac{3}{2}$.

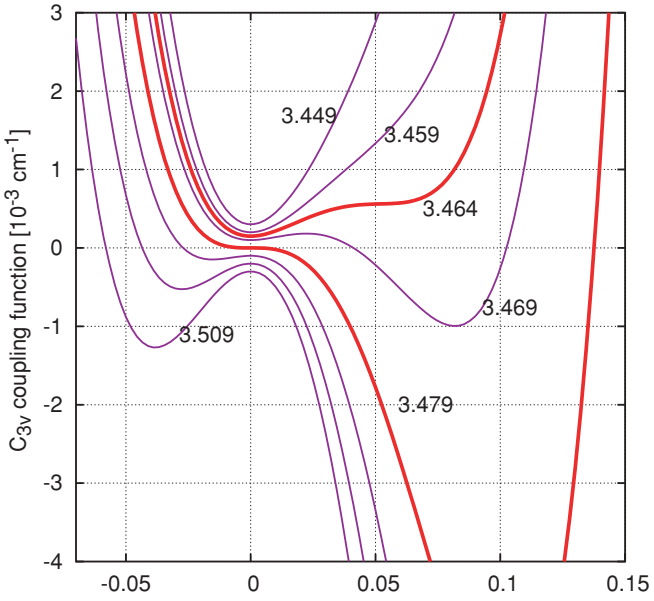

FIG. 9. (Color online) C_{3v} coupling function for stretching modes (ν_1,ν_3) of methane near the ν_1 RE $(x=0)$ for different values $n+6\frac{1}{2}$ of polyad integral $\mathcal{N}$ and $y=0$ $(\phi=0,\pi)$. Each curve is shifted vertically for better comparison; bolder lines mark critical sections.

Additionally, since the reflection symmetry is not broken, we can fix $y=0$, and study the dependence of $\mathcal{H}_n^{C_{3v}}$ on x and parameter n as illustrated in Fig. 9.

The deformation culminates in a more complex event at $\mathcal{N}=3.478$ that creates two new unstable RE with $\phi=0,\pi$ on the D_{2d} sphere, while at the same time, the saddle on the C_{3v} sphere moves through the ν_1 pole to the $\phi=\pi$ semicircle while the pole turns into a maximum; see Fig. 9. So we end up with coupling surfaces in Fig. 7. At sufficiently large n, all newly created RE have minimum energies, while the "original" ν_1 and ν_3 RE evolve toward maximal energies arriving for $n=8$ at the energy gap of 500–1000 cm^{-1}, see Fig. 8. This is comparable to the local-mode well in SiH_4 [20].

Finally, we like to mention a number of bifurcations of these original stretching RE which involve bending modes and change the full eight-degree-of-freedom stability (see respective circles in Fig. 8). In particular, very early at $\mathcal{N}=4.272$, the C_{3v} ν_3 RE goes through a Hopf bifurcation involving both ν_2 and ν_4; later at $\mathcal{N}=10.224$, this RE has a pitchfork bifurcation that involves ν_4. This indicates very clearly that stretching-bending distinction is not globally valid in methane and that the information we acquired in this section on the stretching RE remains incomplete.

4. Dipole active localization

Ignoring bending degrees of freedom, we can, nevertheless, suggest certain localization possibilities and select the ones that induce the largest dipole moment. We consider stable (in the restricted sense) stretching RE. For $n=8$, all original stretching RE, are stable and furthermore, we have stable RE among newly created ones at bottom energies. We notice immediately, that the ν_1 RE and the D_{2d} ν_3 RE (maximum energy in Fig. 8) cannot induce any dipole moment. At the same time, because of the shallow valley geometry of the coupling surfaces (Fig. 7), stretching localization near one of the new low-energy RE is incomplete; it resembles that of a hindered one-dimensional rotor. It follows that the most simple candidate to explore below in Sec. IV is the C_{3v} $(\phi=\pi)$ ν_3 RE. We further note that (in polyads P_2 and P_4) the overtones of ν_3 are known to be the states with strongest absorption, and that motion along the C_{3v} RE results in the most significant electric dipole moment oscillations.

We note (cf. Fig. 16 of Ref. [3] for $C_{3v}\times\mathcal{T}$) that unlike the ν_1 RE and the D_{2d} ν_3 RE, which are essentially just normal modes ν_1 and ν_3, the C_{3v} ν_3 RE is a specific nonlinear normal mode with zero angular momentum. In the configuration space $\mathbb{R}^3$ of the normal ν_3 displacements, it corresponds to vibrations along one of the four C_3 axes of the tetrahedron. As a consequence, the respective localized state is four times (quasi)degenerate, just as the local mode to which this RE is smoothly connected.

IV. INTENSITY OF SINGLE PHOTON TRANSITIONS $P_0 \to P_n$ WITH LARGE n

In this section, we consider the description of the intensity of the direct transition $P_0 \to P_n$, and in particular, we like to understand its dependence on the polyad number n. For sufficiently large n, this can be done semiclassically.

We pursue two approaches. In the model approach, we try to reduce the analysis to a single dimension corresponding to the polyad degree of freedom. We select a predominant direction of the dipole active distortion of the molecule along a stable RE. Following subsection III C4, we focus on the C_{3v} RE. In a more general approach, we investigate the possibility to rewrite the dipole moment operator in such a way that the polyad degree of freedom becomes separated.

We also explore the origins of the terms in the polyad dipole moment. Using the normalizing transformation $(Q,P)\mapsto(q,p)$ introduced in subsection III A, we express the original vibrationally induced (oscillating) dipole moment $\mu(Q)$ in the variables (q,p) of the normalized system and obtain the *effective dipole moment* $\mu_{\mathrm{eff}}(q,p)$. For the quantized normalized system, neglecting rotation of the molecule and assuming that the electric field component of the radiation $\mathbf{E}$ and dipole moment $\boldsymbol{\mu}$ are collinear, the probability of the transition $|0\rangle \to |n\rangle$ is proportional to $|\langle 0|\hat{\mu}_{\mathrm{eff}}(q,p)|n\rangle|^2$.

A. One-dimensional Morse oscillator model

The general scheme can be illustrated using a one-dimensional Morse oscillator with Hamiltonian

$$H_{\mathrm{Morse}} = \frac{p_r^2}{2M} + D_e\left[1-\exp\left(-\alpha\frac{r-r_e}{r_e}\right)\right]^2,$$

where parameters D_e, r_e, and α, represent the dissociation energy, the equilibrium distance, and the "strength" of the chemical bond and M is the reduced mass. The Birkhoff normal form for this system

$$\mathcal{H} = \omega_0(N - 2\varepsilon^2 N^2) \tag{5a}$$

is a polynomial[9] of degree 2 in the classical action

$$N = \tfrac{1}{2}(p^2 + q^2) \tag{5b}$$

with the smallness parameter

$$\varepsilon = \tfrac{1}{2}\sqrt{\alpha/r_e}(2D_eM)^{-1/4} \tag{5c}$$

and the frequency

$$\omega_0 = 8D_e\varepsilon^2 \tag{5d}$$

of harmonic oscillations about the equilibrium $r = r_e$. Taylor expanding the canonical transformation that brings the system to this normal form gives for $Q = r - r_e$

$$Q \mapsto 2\varepsilon\frac{r_e}{\alpha}\left(q + \varepsilon(q^2 + 2p^2) + \frac{\varepsilon^2}{2}(5q^2/3 - p^2)q + \cdots\right).$$

Rewriting the first (linear) term of the vibrationally induced dipole moment $\mu(Q) = \mu_1 Q + \cdots$, in terms of the dynamical variables (q,p) of the normalized system, and quantizing the latter, we compute the matrix element

$$\langle 0|\mu_{\text{eff}}|n\rangle = \mu_1\frac{r_e}{\alpha}\varepsilon^n(-1)^{n-1}\frac{\sqrt{2^n n!}}{n} \tag{6}$$

that describes the transition $|0\rangle \to |n\rangle$.

B. Generalization to the multidimensional case

The motion along the classical $\mathbb{S}^1$ orbits defined by the polyad integral $\mathcal{N}$ can be associated with a 1D anharmonic oscillator system, such as the Morse oscillator in subsection IV A. If this motion corresponds to an RE and the latter is an elliptic orbit stable enough for quantum localization to occur, the induced dipole moment for the localized states will be defined primarily by the deformations of the molecule associated to the particular classical RE. The system becomes, therefore, essentially one-dimensional and we can use the results of the previous section, namely Eq. (6) with n treated as the value of $\mathcal{N}$.

Polyads of the CH_4 molecule were approximated globally in Ref. [52] using a one-dimensional Morse oscillator with frequency which is naturally close to that of bending vibrations (1582 cm^{-1} for ν_2 and 1367 cm^{-1} for ν_4 [53]). However, the 1:2 resonance makes the situation singular. Because of the resonance, any purely stretching RE is "short", i.e., its frequency ω_0 is twice that of the $\mathcal{N}$ motion. Furthermore, if we double the polyad frequency when working with such an RE, then in Eq. (6) we should also use the number of stretching quanta $n/2$ instead of the polyad number n. For the $C_{3v} \times \mathcal{T}$ ν_3 RE of the CH_4 molecule we can use the following values (in cm^{-1}, atomic units, and debyes)

μ_1	0.352 [54], 0.390 [53] D/a_0 (for ν_3),
D_e	35000 [9] or 37360 [52] cm^{-1},
ω_0	2×1563.6 [52] or 3095 [53] cm^{-1},
ε	$\approx$0.10 (from D_e, and ω_0),
f	0.332 E_h/a_0^2 (ν_3 force constant) [53],
M	0.916 m_u (from f/ω_0^2),
r_e/α	1.0 a_0 (from ε, D_e, and M),

and obtain from Eq. (6) the vibrational transition moment $|\langle\mu\rangle| = |\langle 0|\hat{\mu}_{\text{eff}}(q,p)|n/2\rangle|$ for the $0 \to P_n$ transitions (see Table IV). Below we use these values to give estimates of the intensity of the most prominent lines in the rotationally resolved $0 \to P_n$ bands with $n = 8,10,12$.

The cross section for a single absorption line

$$\sigma(\nu) = 2\pi^2|\langle\mu\rangle|^2(3\eta\varepsilon_0 ch)^{-1}F(T,J)\nu g(\nu - \nu_0)$$

includes dielectric constant $\eta \approx 1$, line form factor $g(\nu - \nu_0)$, and factor $F(T,J)$ that accounts for the population of the lower state with a given angular momentum J, degeneracy of that state, and rotational matrix elements. At the resolution of 0.04 cm^{-1}, we may assume that the fine structure of the J multiplet caused by the tensorial centrifugal distortion remains unresolved and that consequently, $F(T,J)$ includes the sum over the components of a single multiplet. For our purposes, we may also further simplify $F(T,J)$ by using the total degeneracy of the multiplet in place of exact rotational and nuclear spin factors, so that

$$F(T,J) \approx (2J+1)^2\exp(-J(J+1)T_r/T)Q(T)^{-1},$$

where $T_r = hcB/k \approx 7.54$ K and the partition function $Q(T)$ can be approximated by Eq. (3) of Ref. [55]. For $T =$ 295 K, the $J = 6$ multiplet is most populated and we have $F(295,6) \approx 0.1$. Assuming a Lorentzian form factor with full width at half maximum (FWHM) = 0.04 cm^{-1} being about the minimal collisional line width observed, and taking its value $(\pi\text{FWHM}/2)^{-1}$ at the center frequency of the spectral line, we arrive at the values for σ in Table IV.

Integral absolute band strengths S_{band} of the unresolved $0 \to P_n$ bands with $n = 8,10,12$ where estimated experimentally in Refs. [25,27,56,57]. Lucchesini and Gozzini [26] determined cross sections σ_{line} for individual rotational lines in the weak 840-nm band, a satellite of the main $0 \to P_8$ transition at 889 nm. Comparing their data to the respective S_{band} value and assuming similar $\sigma_{\text{line}}/S_{\text{band}}$ ratio for $n =$ 10,12, gives σ_{line} values of the same order as those in Table IV.

TABLE IV. Estimated absorption cross sections σ of the most intense rotational transitions in the $0 \to P_n$, $n = 8,10,12$ bands of methane for $T = 295$ K and full width at half maximum = 0.04 cm^{-1}.

n	ν (cm^{-1})	$\lvert\langle\mu\rangle\rvert$ (D)	σ (cm^2/mol)
8	11 300	2.3×10^{-4}	3.7×10^{-22}
10	13 760	6.1×10^{-5}	3.2×10^{-23}
12	16 135	1.8×10^{-5}	3.5×10^{-24}

[9] In quantum mechanics, we have $N = n + \frac{1}{2}$ and the closed normal form in Eq. (5a) corresponds to the well known exact solution for the Morse oscillator system.

This suggests the utility of Eq. (6) for crude estimates. This also indicates that our experiment (Sec. II) with the estimated minimal cross section of 10^{-26} cm^2 per molecule had a good margin of sensitivity even in the case of $0 \to P_{12}$ and that observing rotational structure of the $0 \to P_{14}$ band should be within reach of contemporary techniques.

C. Model transition moment for CH_4

One of the most frustrating problems in the traditional Taylor series–based spectroscopic approach [5,6] to the analysis of direct transitions $P_0 \to P_n$ with large $n \approx 10$ is the absence of any clues as to the possible values of the parameters of the effective transition moment μ_{eff} induced by the vibrations. In such analysis, both the effective polyad Hamiltonian $\mathcal{H}$ and dipole moment μ_{eff} are Taylor expanded near the equilibrium, and as the work progresses to states in higher excited polyads, higher degrees in both series get involved and their coefficients are determined. However, there is a profound difference between the way in which $\mathcal{H}$ and μ_{eff} are extrapolated. The lower degree terms of $\mathcal{H}$ can be determined from the analysis of lower polyads, notably P_3 and P_4, and can be used subsequently to predict—with varying accuracy—the higher excited states. Not so for μ_{eff}: in this traditional approach, in order to describe $P_0 \to P_n$, we have to inject new terms of specific degrees. For large number K of the vibrational degrees of freedom involved in the polyads, the number of terms to be injected can be quite significant (subsection IV C1).

It is clear that any spectroscopic analysis of $P_0 \to P_n$ with large n would require rough initial values of the parameters in μ_{eff}. At the contemporary level of *ab initio* calculations, there is little hope to obtain anything beyond cubic and maybe quartic terms in μ_{eff}. Therefore, we should use more information on the dynamics of the system to confine our description to a smaller number of quantum states which would require smaller number of phenomenological parameters (subsection IV C2). We should also think of rewriting μ_{eff} in such a way that it can be extrapolated similarly to $\mathcal{H}$.

1. *Number of linearly independent terms in* μ_{eff}

Recall that in the case of tetrahedral symmetry, $\mu_{\text{eff}} = \mu_{\text{eff}}^{F_2}$ transforms like any polar three-vector according to the irreducible representation F_2. So within the usual framework, $P_0 \to P_n$ is described by terms of type F_2 of degree at least $n/2$ or higher in creation operators a^+. For example, the term $(a_1^+)^3 a_3^+$ describes the $P_0 \to 3\nu_1 + \nu_3$ transition suggested in Refs. [21,22]. Clearly, there are much more such terms of degree 4, let alone those of higher degrees that involve bending modes, and the coefficients in front of them are unknown and cannot be derived from the studies of lower polyads.

All terms in $\mu_{\text{eff}}^{F_2}$ describing the $P_0 \to P_n$ transition without recombinations, i.e., terms consisting purely of z (or of creation operators a^+), are described by the generating function

$$g_\mu = \frac{(t_2^2 + t_2 + 1)(t_3^2 + t_3 + 1)(t_4^2 + t_4 + 1)\chi}{D_1 D_2 D_3 D_4}$$

of four formal variables (t_1,t_2,t_3,t_4) representing normal mode coordinates z_1, $z_{2,3}$, $z_{4,5,6}$, and $z_{7,8,9}$, respectively. The numerator of g_μ with

$$\begin{aligned}\chi = {} & t_4 + t_3 - t_3 t_4 + (t_3 + t_4 + t_2) t_3 t_4 \\ & + t_3 t_4 (t_4^2 + t_3^2) + t_2 t_3 t_4 (t_3 + t_4) + t_2 t_3^3 + t_2 t_4^3 \\ & + t_3^3 t_4^2 + t_3^2 t_4^3 - t_2 t_3 t_4 (t_3^2 + t_4^2) \\ & + t_2 t_4^4 t_3 + t_2 t_3^4 t_4 + t_2 t_3^2 t_4^3 + t_2 t_3^3 t_4^2 - t_3^3 t_4^3 \\ & + (t_4 + t_3 + t_2) t_3^3 t_4^3\end{aligned}$$

represents F_2-type covariants; the denominator terms

$$\begin{aligned} D_1 &= 1 - t_1 \\ D_2 &= (1 - t_2^2)(1 - t_2^3) \\ D_3 &= (1 - t_3^2)(1 - t_3^3)(1 - t_3^4) \\ D_4 &= (1 - t_4^2)(1 - t_4^3)(1 - t_4^4) \end{aligned}$$

describe principal totally symmetric (type A_1) invariants. Taylor expanding g_μ and collecting terms $t_1^{k_1} t_2^{k_2} t_3^{k_3} t_4^{k_4}$ with $2k_1 + k_2 + 2k_3 + k_4 = n$ gives a formal representation of the $P_0 \to P_n$ effective dipole moment. Each monomial represents a particular type of linearly independent F_2 covariants; coefficients in front of the monomials indicate the number of covariants of the particular type.

If $\mu_{\text{eff}}^{F_2}$ is analytic, then terms of higher relative degree in t_1 and t_3 are of lower total degree and make, therefore, a more important contribution to μ_{eff} and to the intensity of the $P_0 \to P_n$ transition. For even polyads, the most important terms in μ_{eff} contain only stretching variables t_1 and t_3. Thus we have

Polyad	Stretching part of μ_{eff}
P_6	$t_1^2 t_3 + t_1 t_3^2 + 2t_3^3$
P_8	$t_1^3 t_3 + t_1^2 t_3^2 + 2t_1 t_3^3 + 2t_3^4$
P_{10}	$t_1^4 t_3 + t_1^3 t_3^2 + 2t_1^2 t_3^3 + 2t_1 t_3^4 + 4t_3^5$
P_{12}	$t_1^5 t_3 + t_1^4 t_3^2 + 2t_1^3 t_3^3 + 2t_1^2 t_3^4 + 4t_1 t_3^5 + 4t_3^6$

Further interpretation of these expressions and explicit construction of the purely stretching terms is relatively simple because powers of t_1 represent essentially a trivial factor. It follows that we should construct all F_2-type covariants of a given degree in $z_{4,5,6}$, see next subsection IV C2, Table V, and Ref. [58]. For odd n, the most important $P_0 \to P_n$ terms in μ_{eff} are, necessarily, of degree 1 in one of the bending variables t_2 or t_4. To find the number of required phenomenological parameters, we should sum up all coefficients in the Taylor expansion. Below we give these numbers for the number of all terms, purely stretching terms, and purely ν_3 terms (the two latter have degree 1 bending contribution for odd polyads).

Polyad	P_1	P_2	P_3	P_4	P_5	P_6	P_7	P_8	P_9	P_{10}	P_{11}	P_{12}
Total	1	3	8	20	43	90	169	313	540	917	1480	2356
ν_1,ν_3	(1)	1	3	2	7	4	14	6	24	10	38	14
ν_3	(1)	1	2	1	4	2	7	2	10	4	14	4

We can see that the total number of possible parameters grows rapidly beyond reasonable. But even the number of purely stretching parameters is relatively large, given that their values are completely unknown. For example, for the analysis of $P_0 \to P_{10}$ within the STDS [4–6] framework, we should "guess" the values of four parameters of purely ν_3 terms, and,

TABLE V. Terms in the transition dipole moment of degree 3 and 4 for excitations of the stretching RE of symmetry $C_{3v} \times \mathcal{T}$.

Degree	Term	g_μ	STDS tensor definition [4–6]		Coefficient
ξ^3	μ_{113}	$t_1^2 t_3$	$z_1^2\ \mu_3^{F_2}$		$12\ \eta_1(1-\eta_1)^{1/2}$
	μ_{133}	$t_1 t_3^2$	$z_1\ [\mu_3^{F_2},\mu_3^{F_2}]^{F_2}$		$12\ \eta_1^{1/2}(1-\eta_1)\sqrt{2}$
	$\mu^{\Gamma}_{(33)3}$	t_3^4	$[[\mu_3^{F_2},\mu_3^{F_2}]^{\Gamma},\mu_3^{F_2}]^{F_2}$	$\Gamma=A_1$	$4\ (1-\eta_1)^{3/2}\sqrt{3}$
				$\Gamma=F_2$	$8\ (1-\eta_1)^{3/2}$
ξ^4	μ_{1113}	$t_1^3 t_3$	$z_1^3(z_4,z_5,z_6) = z_1^3\mu_3^{F_2}$		$-16\eta_1^{3/2}(1-\eta_1)^{1/2}$
	μ_{1133}	$t_1^2 t_3^2$	$z_1^2\ [\mu_3^{F_2},\mu_3^{F_2}]^{F_2}$		$-24\eta_1(1-\eta_1)\sqrt{2}$
	$\mu^{\Gamma}_{1(33)3}$	$t_1 t_3^3$	$z_1[[\mu_3^{F_2},\mu_3^{F_2}]^{\Gamma},\mu_3^{F_2}]^{F_2}$	$\Gamma=A_1$	$-16\eta_1^{1/2}(1-\eta_1)^{3/2}\sqrt{3}$
				$\Gamma=F_2$	$-32\eta_1^{1/2}(1-\eta_1)^{3/2}$
	$\mu^{\Gamma F_2}_{(33)(33)}$	t_3^3	$[[\mu_3^{F_2},\mu_3^{F_2}]^{\Gamma},[\mu_3^{F_2},\mu_3^{F_2}]^{F_2}]^{F_2}$	$\Gamma=A_1$	$-8\sqrt{6}(1-\eta)^2$
				$\Gamma=F_2$	$-8\sqrt{2}(1-\eta)^2$

if ν_1 is also important, another six parameters. We address this problem in the next section.

2. *RE-induced dipole moment*

The number of terms in μ_{eff} becomes so large that we need a model of what goes on. In subsection III C4 we selected the $C_{3v} \times \mathcal{T}$ stretching RE for the analysis. Here we assume that the bright state of the $P_0 \to P_n$ transition is localized near this RE. Let $Z = Z_{C_{3v}}(\eta(n),\phi(n))$ define such RE on P_n in the form (4). Let $(\xi,\bar{\xi})$ be coordinates along the axis defined by Z in the original phase space. Then we can represent μ as mainly a power series in $(\xi,\bar{\xi})$. At first, we can neglect all other small terms in that series.

To have a simple example, let us assume no bending content ($\eta_2 = \eta_4 = 0$) in Z, and let us fix the remaining phase $\phi_1 = \pi$ as in Ref. [20] and denote $\eta_1 = \eta(n)$. Let us also distinguish the four different equivalent $C_{3v} \times \mathcal{T}$ RE by vector subscripts

$$\alpha = (1,1,1),\quad (-1,-1,1),\quad (1,-1,-1),\quad (-1,1,-1),$$

one for each of the four axes C_3 in Fig. 2. Then according to Eq. (4) we have

$$Z_\alpha = \sqrt{n}\left(-\sqrt{\eta},(0,0),\sqrt{1-\eta}\,\frac{\alpha}{\sqrt{3}},(0,0,0)\right)$$

and therefore

$$\xi_\alpha(z) = -\sqrt{\eta}z_1 + \sqrt{\frac{1-\eta}{3}}\alpha(z_4,z_5,z_6)^T.$$

Vectors ξ_α represent distortions caused by four stretching RE of the system. In order to reach polyad P_{2s}, we should excite either one of them by s stretching quanta in a row. This means that μ should include terms ξ_α^s. Once this is understood, all we have to do is to construct components of the three-vector μ^{F_2} (with respect to coordinate axes in Fig. 2) by combining the monomials ξ_α^s appropriately. To this end, we note that ξ_α^s with $s = 1,2,3,\ldots$ are permuted by the operations of T_d in the same way as ξ_α. Therefore,[10] we can combine four ξ_α^s in the same way as four ξ_α in order to obtain the three components of vector

$$\mu^{F_2} = \begin{pmatrix} +1 & -1 & +1 & -1 \\ +1 & -1 & -1 & +1 \\ +1 & +1 & -1 & -1 \end{pmatrix} \begin{pmatrix} \xi^s_{(1,1,1)} \\ \xi^s_{(-1,-1,1)} \\ \xi^s_{(1,-1,-1)} \\ \xi^s_{(-1,1,-1)} \end{pmatrix}.$$

Substituting expressions for ξ_α and expanding, we express μ^{F_2} in terms of normal mode coordinates z_k. The result may have several terms but it depends on a single mixing parameter $\eta = \eta_1$. Specifically, for each degree s in z, we can express $\mu^{F_2}(z,\eta)$ as a linear combination of STDS tensor operators [4–6] constructed from $z_1^{A_1} = z_1$ and $\mu_3^{F_2} = (z_4,z_5,z_6)$. Results for $s = 3$ and $s = 4$ are given in Table V. Thus for $s = 4$, the dipole moment $\mu^{F_2}(z,\eta)$ can be expressed using six tensors, while for $s = 3$ we use four tensors. Replacing z_k by quantum creation operators a_k^+, we arrive at the wanted quantum transition moment operator $\hat{\mu}^{F_2}$.

Note that the formal tensor construction of powers $[\mu_3^{F_2}]^s$ in Table V with all possible intermediate irreducible representations Γ gives redundancies. $\Gamma = A_2$ and F_1 are excluded automatically because, obviously, only even powers, i.e., invariant with respect to permutations, can be built. Furthermore, the number of linearly independent terms of degree s and symmetry type F_2, which can be constructed from $\mu_3^{F_2}$ is given by the coefficients in front of the respective powers in the Taylor expansion of the generating function [58]

$$g_3^{F_2}(t_3) = \left(t_3 + t_3^2 + t_3^3\right)/D_3 = t_3 + t_3^2 + 2t_3^3 + 2t_3^4 + \cdots$$

So there are only two cubic and two quartic terms and in each case, among three possibilities with $\Gamma = A_1,E,F_2$ one should be excluded, i.e., one coefficient should be set exactly to 0. In Table V, we have chosen to exclude $\Gamma = E$.

Furthermore, our results in subsection III C1 suggest that, unlike in a local mode system, the ν_1 content in the $C_{3v} \times \mathcal{T}$ RE

[10]This is equivalent to projecting ξ_α^s on the rows of the irreducible representation F_2.

of CH_4 remains low (about 1% for $n = 8$). Consequently, terms of nonzero degrees in $\eta_1^{1/2}$ are strongly discriminated and can be neglected. This contradicts the hypothesis of Boraas *et al.* [21,22] which implies high ν_1 content and which was made largely for the sake of simplifying tentative line assignments.

V. DISCUSSION AND RESULTS

At the base of all contemporary, extremely sophisticated, attempts [5,7,8] to analyze spectroscopic data on excited rovibrational states of methane (and similar systems) is the Taylor expansion in dynamical variables (q, p) at the equilibrium. Clearly, this becomes increasingly inadequate as we ascend higher up in energy both in terms of convergence and the sheer number of parameters. We believe that progress will not always be possible through accumulation of computer power and models that stem essentially from 1930s. In this work, we attempted to investigate alternatives and complementary approaches and to foresee the future of this field. The idea is to uncover a small part of the polyad P_n, which is distinguished dynamically and is visible in the $P_0 \rightarrow P_n$ experiment, and to confine the analysis accordingly.

A. Vibrational localization in methane

One of our principal objectives was understanding vibrational localization in higher polyads which would allow selecting a small group of excited vibrational states that we observe. We have not resolved this problem definitely for several reasons: low cutoff in the Taylor series for the vibrational Hamiltonian, restriction to purely stretching modes, and neglect for rotation-vibration interactions. Indeed, our present analysis relied on the purely vibrational quartic Hamiltonian $\mathcal{H}$. From Table II, we can see that several terms in $\mathcal{H}^2$, notably $t^{A_1}_{3333}$ and t_{1313} describing stretching modes, are excessively large and that such $\mathcal{H}$ can hardly be considered as a well-behaving converged series. So information on higher-degree terms from spectroscopic sources [7,8], *ab initio* predictions [14,59,60], and Morse potential models should be incorporated. We have seen that bending modes were involved in a number of bifurcations of stretching RE and cannot therefore be disregarded. Finally, methane has relatively large rotational constant B and strong rotation-vibration interactions which cause, in particular, mixing of vibrational modes. The most important lowest order Coriolis interactions of type $[q \times p] \cdot j$ may result in bending-stretching mixing, higher-order terms may couple stretching modes. All these aspects can be incorporated in our analysis without any significant extensions of the theory and will result in a more reliable description of the RE structure of polyads and in extending this description by an additional parameter, the amplitude of the total angular momentum j.

B. Interpretation of the $P_0 \rightarrow P_n$ spectra

Traditionally, the $P_0 \rightarrow P_8$ transition was assigned to an overtone of the fully symmetric stretch ν_1 and one quantum of the dipole active ν_3 mode. The most plausible explanation of the $P_0 \rightarrow P_n$ spectra that we have come up with as a result of the present study is quite different. We proposed a concrete vibrational assignement in terms of vibrational relative equilibria and explain it. Of nine vibrational degrees of freedom we suggest focusing on a particular one, which is, however, neither a naive normal mode overtone, nor a simple "local mode" (LM) vibration of a particular chemical bond C–H.

We believe that our $P_0 \rightarrow P_n$ spectra involve a small group (cluster) of bright and dark upper states localized near the $C_{3v} \times \mathcal{T}$ $n\nu_3$ RE. Because we deal with the same isotropy as in the case of LM's, the number of states and the symmetry properties of the cluster are the same. We have four states split into an $A_1 + F_2$ doublet, in which the A_1 component is dark (in the absence of rotation) and the F_2 component is active. Unlike the LM states, however, the ν_1 content is negligible.

Comparing to the $(n-1)\nu_1 + \nu_3$ assignment we may note a number of strong points in our favor. Most importantly, a transition to an appropriate C_{3v} localized $n\nu_3$ state is likely to be by orders of magnitude stronger than $(n-1)\nu_1 + \nu_3$. Furthermore, because it involves vibrations about the ν_1 RE, the $(n-1)\nu_1 + \nu_3$ state is less likely to be localized and less likely to have such a simplistic normal mode characteristics. Further clarification of this situation can be given after computing stability of the RE in question and frequencies of oscillations about them.

Returning to our proposed assignment, it can be tested in a number of ways. A complete rovibrational polyad computation of the $0 \rightarrow P_n$ spectrum (using, for example, the STDS program [4–6]) with the dipole moment in subsection IV C2 may be attempted and the vibrational states that become involved in the transition may be identified subsequently. Such computation requires considerable resources but is technically possible. In the simplest approximation for even polyad numbers n, one may attempt to interpret the involved states as part of a purely $n\nu_3$ stretching polyad localized near the C_{3v} RE (and thus follow the older work [3,50]). Such localized states would constitute a cluster of four states composed of states with smallest value of the vibrational angular momentum l. For even and odd n, this would involve $l = 0,2$ and $l = 1,3$, respectively. Computations in such approach become less heavy. One should note, however, that the rest of the $n\nu_3$ states has to be disregarded since entire isolated stretching polyads do not exist in methane. Finally, it may be possible to reproduce the rotational structure of such states using an appropriate effective rotational Hamiltonian of a four-well C_{3v} symmetric top. This should be similar to the local mode formalism of Ref. [28], albeit the wells do not correspond to the four C–H local modes but are formed by the ν_3 mode alone.

Prior to such attempts, we should follow the outline in subsection III C and demonstrate more convincingly that the localization of the $C_{3v} \times \mathcal{T}$ ν_3 type does indeed occur. If that is confirmed, it is quite likely that the individual rovibrational transitions reported in Sec. II can be interpreted satisfactorily on the basis of our vibrational assignment and treated subsequently within a standard spectroscopic approach.

ACKNOWLEDGMENTS

We thank B. I. Zhilinskií for discussions and encouragement; we are grateful to V. Boudon for drawing our attention to this problem and for exchanges concerning the $P_0 \rightarrow P_8$ spectra. D. N. Kozlov was supported by the visiting professor program of the Région Nord–Pas-de-Calais. Part of this work was supported by the Russian Foundation for Basic Research (RFBR), grant number 07–02–01097, the Swiss Federal Office of Energy and the Swiss National Science Foundation.

[1] D. N. Kozlov and P. P. Radi, J. Raman Spectrosc. **39**, 730 (2008).

[2] See supplementary material at [http://link.aps.org/supplemental/10.1103/PhysRevA.82.012503] [includes a compressed archive of raw LIG absorption spectra of $P_0 \rightarrow P_{10}$ (p10_124 K_187 mbar, 116 Kb) and $P_0 \rightarrow P_{12}$ (p12_124K_200 mbar, 163Kb) bands displayed in Fig. 3 and 4, respectively].

[3] K. Efstathiou, D. A. Sadovskií, and B. I. Zhilinskií, SIAM J. Appl. Dyn. Syst. (SIADS) **3**, 261 (2004).

[4] J.-P. Champion, M. Loëte, and G. Pierre, in *Spectroscopy of the Earth's Atmosphere and Interstellar Medium*, edited by K. N. Rao and A. Weber (Academic Press, San Diego, 1992).

[5] C. Wenger and J.-P. Champion, J. Quant. Spectrosc. Radiat. Transf. **59**, 471 (1998).

[6] J.-P. Champion, Ch. Wenger, and V. Boudon, *Spherical Top Data System (STDS): a computer package for simulation of spherical top spectra*, developed and maintained at the Université du Bourgogne, Dijon, [http://icb.u-bourgogne.fr/OMR/SMA/SHTDS/STDS.html].

[7] V. Boudon, M. Rey, and M. Loëte, J. Quant. Spectrosc. Radiat. Transf. **98**, 394 (2006).

[8] S. Albert, S. Bauerecker, V. Boudon, L. R. Brown, J.-P. Champion, M. Loëte, A. Nikitin, and M. Quack, Chem. Phys. **356**, 131 (2009).

[9] R. van Harrevelt, J. Chem. Phys. **125**, 124302/1 (2006).

[10] L. Halonen, J. Chem. Phys. **106**, 831 (1997).

[11] R. Marquardt and M. Quack, J. Chem. Phys. **109**, 10628 (1998).

[12] E. Venuti, L. Halonen, and R. G. D. Valle, J. Chem. Phys. **110**, 7339 (1999).

[13] R. Lemus and A. Frank, J. Mol. Spectrosc. **201**, 198 (2000).

[14] X.-G. Wang and E. L. Sibert III, Spectrochim. Acta, Part A **58**, 863 (2002).

[15] R. Marquardt and M. Quack, J. Phys. Chem. A **108**, 3166 (2004).

[16] J. Montaldi, M. Roberts, and I. Stewart, Philos. Trans. R. Soc. London A **325**, 237 (1988).

[17] J. Montaldi, M. Roberts, and I. Stewart, Nonlinearity **3**, 695 (1990).

[18] J. Montaldi, M. Roberts, and I. Stewart, Nonlinearity **3**, 731 (1990).

[19] D. A. Sadovskií, N. G. Fulton, J. R. Henderson, J. Tennyson, and B. I. Zhilinskií, J. Chem. Phys. **99**, 906 (1993).

[20] H. Crogman, V. Boudon, and D. A. Sadovskií, Eur. Phys. J. D **42**, 61 (2007).

[21] K. Boraas, D. F. De Boer, Z. Lin, and J. P. Reilly, J. Chem. Phys. **99**, 1429 (1993).

[22] K. Boraas, Z. Lin, and J. P. Reilly, J. Chem. Phys. **100**, 7916 (1994).

[23] T. Tsukamoto and H. Sasada, J. Chem. Phys. **102**, 5126 (1995).

[24] A. Campargue, D. Permogorov, and R. Jost, J. Chem. Phys. **102**, 5910 (1995).

[25] J. J. O'Brien and H. Cao, J. Quant. Spectrosc. Radiat. Transfer **75**, 323 (2002).

[26] A. Lucchesini and S. Gozzini, J. Quant. Spectrosc. Radiat. Transfer **103**, 209 (2007).

[27] L. P. Giver, J. Quant. Spectrosc. Radiat. Transfer **19**, 311 (1978).

[28] L. Halonen and M. S. Child, Comput. Phys. Commun. **51**, 173 (1988).

[29] M. Chevalier, A. D. Martino, and F. Michelot, J. Mol. Spectrosc. **131**, 382 (1988).

[30] C. Leroy and F. Michelot, J. Mol. Spectrosc. **151**, 71 (1992).

[31] C. Leroy, F. Michelot, and V. Boujut, J. Mol. Spectrosc. **173**, 333 (1995).

[32] L. E. Fried and G. S. Ezra, J. Chem. Phys. **86**, 6270 (1987).

[33] L. Xiao and M. E. Kellman, J. Chem. Phys. **90**, 6086 (1989).

[34] Z.-M. Lu and M. E. Kellman, J. Chem. Phys. **107**, 1 (1997).

[35] C. Jaffé, J. Chem. Phys. **89**, 3395 (1988).

[36] M. E. Kellman, J. Chem. Phys. **93**, 6630 (1990).

[37] M. E. Kellman and G. Chen, J. Chem. Phys. **95**, 8671 (1991).

[38] M. P. Jacobson, C. Jung, H. S. Taylor, and R. W. Field, J. Chem. Phys. **111**, 600 (1999).

[39] M. I. El Idrissi, B. I. Zhilinskií, P. Gaspard, and M. Herman, Mol. Phys. **101**, 595 (2003).

[40] I. N. Kozin, D. A. Sadovskií, and B. I. Zhilinskií, Spectrochim. Acta, Part A **61**, 2867 (2005).

[41] D. A. Sadovskií and B. I. Zhilinskií, J. Chem. Phys. **103**, 10520 (1995).

[42] M. V. Karasev and V. P. Maslov, Theor. Math. Phys. **53**, 1186 (1982).

[43] Y. M. Vorob'ev and M. V. Karasev, Dokl. Akad. Nauk USSR **297**, 1294 (1987).

[44] M. V. Karasev (ed.), *Coherent Transform, Quantization, and Poisson Geometry* (American Mathematical Society, Providence, RI, 1998), Vol. 187.

[45] A. Weinstein, Invent. Math. **20**, 47 (1973).

[46] J. Moser, Commun. Pure Appl. Math. **29**, 727 (1976).

[47] V. I. Arnol'd, *Mathematical Methods of Classical Mechanics*, 2nd ed., Springer Graduated Texts in Mathematics Vol. 60 (Springer-Verlag, New York, 1989), translated from Russian by K. Vogtmann and A. Weinstein.

[48] V. I. Arnol'd, V. V. Kozlov, and A. I. Neíshtadt, *Mathematical Aspects of Classical and Celestial Mechanics. Dynamical Systems III*, Encyclopedia of Mathematical Sciences Vol. 3 (Springer-Verlag, Berlin, 1986).

[49] J. Montaldi and R. M. Roberts, J. Nonlinear Sci. **9**, 53 (1999).

[50] B. I. Zhilinskií, Chem. Phys. **137**, 1 (1989).

[51] L. Michel and B. I. Zhilinskií, Phys. Rep. **341**, 11 (2001).

[52] C. Wenger, J. P. Champion, and V. Boudon, J. Quant. Spectrosc. Radiat. Transfer **109**, 2697 (2008).

[53] A. Mourbat, A. Aboumajd, and M. Loëte, J. Mol. Spectrosc. **190**, 198 (1998), see Table 3 on p. 202.

[54] D. P. Chong and D. Papousek, Chem. Phys. Lett. **193**, 399 (1992), see Table 1 and 2 on p. 400.

[55] R. S. McDowell, J. Quant. Spectrosc. Radiat. Transfer **38**, 337 (1987).

[56] E. K. Lewis, C. J. Moehnke, and C. E. Manzanares, Chem. Phys. Lett. **394**, 25 (2004).

[57] Y. Perez-Delgado, E. K. Lewis, C. J. Moehnke, M. C. Salazar, A. J. Hernandez, and C. E. Manzanares, Mol. Phys. **107**, 1367 (2009).

[58] B. I. Zhilinskií, *Theory of Complex Molecular Spectra* (Moscow State University Press, Moscow, 1989). [in Russian]

[59] D. W. Schwenke, Spectrochim. Acta, Part A **58**, 849 (2002).

[60] D. W. Schwenke and H. Partridge, Spectrochim. Acta, Part A **57**, 887 (2001).